Intelligent and Converged Networks
2021, 2(1): 30–49

ISSN 2708-6240
DOI: 10.23919/ICN.2020.0018

Revisiting the nonlinear Gaussian noise model for hybrid fiber spans

Ioannis Roudas*, Jaroslaw Kwapisz, and Xin Jiang

Abstract: We rederive from first principles and generalize the theoretical framework of the nonlinear Gaussian noise model to the case of coherent optical systems with multiple fiber types per span and ideal Nyquist spectra. We focus on the accurate numerical evaluation of the integral for the nonlinear noise variance for hybrid fiber spans. This task consists in addressing four computational aspects: (1) Adopting a novel transformation of variables (other than using hyperbolic coordinates) that changes the integrand to a more appropriate form for numerical quadrature; (2) Evaluating analytically the integral at its lower limit, where the integrand presents a singularity; (3) Dividing the interval of integration into subintervals of size π and approximating the integral over each subinterval by using various algorithms; and (4) Deriving an upper bound for the relative error when the interval of integration is truncated in order to accelerate computation.

We apply the proposed analytical model to the performance evaluation of coherent optical communications systems with hybrid fiber spans composed of quasi-single-mode and single-mode fiber segments. More specifically, the model is used to optimize the lengths of the optical fiber segments that compose each span in order to maximize the system performance. We check the validity of the optimal fiber segment lengths per span provided by the analytical model by using Monte Carlo simulation, where the Manakov equation is solved numerically using the split-step Fourier method. We show that the analytical model predicts the lengths of the optical fiber segments per span with satisfactory accuracy so that the system performance, in terms of the *Q*-factor, is within 0.1 dB from the maximum given by Monte Carlo simulation.

Key words: nonlinear Gaussian Noise (GN) model; perturbation theory; hybrid fiber spans

1 Introduction

One of the most important theoretical achievements of recent years in optical telecommunications was the approximate solution of the nonlinear Schrödinger equation[1] and its vector counterpart, the Manakov equation[2]. More specifically, many alternative analytical formalisms, e.g., Refs. [3–14], have been proposed for the estimation of the impact of distortion due to Kerr nonlinearity on the performance of coherent optical communications systems with no inline dispersion compensation. Among those, the nonlinear Gaussian noise model (see Refs. [7, 9]), was established in the consciousness of the scientific community as an industry standard, due to its relative simplicity compared to other, more sophisticated but more accurate models in Refs. [10, 11], for example.

The nonlinear Gaussian noise model was originally developed for a single fiber type per span, lumped optical

• Ioannis Roudas is with the Department of Electrical and Computer Engineering, Montana State University, Bozeman, MT 59717, USA. E-mail: ioannis.roudas@montana.edu.
• Jaroslaw Kwapisz is with the Department of Mathematical Sciences, Montana State University, Bozeman, MT 59717, USA. E-mail: jarek@math.montana.edu.
• Xin Jiang is with the Department of Engineering and Environmental Science, College of Staten Island, City University of New York, Staten Island, NY 10314, USA. E-mail: jessica.jiang@csi.cuny.edu.
∗ To whom correspondence should be addressed.
Manuscript received: 2020-10-23; accepted: 2020-11-28

amplifiers, and ideal Nyquist spectra[5]. Over the years, it has been constantly revised and has been applied to a variety of system and link configurations, e.g., see Refs. [6, 7, 9, 12, 15–21].

The nonlinear Gaussian Noise-model Reference Formula (GNRF)[9] that provides the power spectral density (psd) of nonlinear noise at the end of the link is general enough to encompass the case of hybrid fiber spans, i.e., fiber spans composed of multiple segments of different fiber types (Fig. 1). However, to the best of our knowledge, the application of the nonlinear Gaussian noise-model to coherent optical communications systems with hybrid fiber spans has hardly received any attention to date. Notable exceptions are the following papers: First, Shieh and Chen[4] studied coherent optical systems with fiber spans consisting of a transmission fiber and a Dispersion Compensation Fiber (DCF). Later on, the papers by Downie et al.[22] and Miranda et al.[23] were dedicated to hybrid spans comprised of quasi-single-mode and single-mode fiber segments. More recent publications by Al-Khateeb et al.[24] and Krzczanowicz et al.[25] focused on hybrid spans for optical phase conjugation[24] and discrete Raman amplification[25], respectively.

The aforementioned publications gave diverse expressions for the nonlinear noise coefficient $\tilde{\gamma}$ used to calculate the nonlinear noise variance $\sigma^2_{\mathrm{NL}} = \tilde{\gamma} P^3$, where P denotes the total average launch power per channel (in both polarizations). Obviously, these formulas for $\tilde{\gamma}$ are interrelated and their apparent dissimilarities are due to the fact that each individual research group studied a different system topology. Their dissimilarities can be also attributed to the use of two slightly different formalisms by different authors, i.e., Refs. [3, 4] and Refs. [7, 9], separately. On most occasions, only final equations for $\tilde{\gamma}$ were provided without any detailed analytical proof, their direct comparison is difficult.

Another issue is that numerical quadrature algorithms for the accurate evaluation of the highly oscillatory integral for the nonlinear noise coefficient $\tilde{\gamma}$ were not discussed in any of the above papers. One reason that no special attention has been devoted to the intricacies of this calculation must be attributed to the fact that a 1 dB error in the nonlinear noise coefficient $\tilde{\gamma}$ results in only 1/3 dB error on optimum effective OSNR[7]. To the best of our knowledge, only Bononi et al.[26] considered in detail the numerical evaluation of the GNRF formula for the case of a single fiber type per span and ideal Nyquist Wavelength Division Multiplexing (WDM) signals.

On a related subject, Poggiolini[7] recommended to truncate the integration region to reduce the computation time of the foregoing numerical quadrature. Since Four-Wave Mixing (FWM) efficiency quickly drops for increasing values of the mixing frequencies f_1 and f_2, it was suggested that one could neglect the integration region beyond where the FWM efficiency dropped below a specified level. However, this issue was not investigated thoroughly in Ref. [7] or in subsequent publications.

This paper is intended to fill the aforementioned gaps in the prior literature. First, to reconcile dissimilar formulas derived before for the nonlinear noise variance of coherent optical communications systems with hybrid fiber spans[4, 22–25], we review and rederive from first principles the theoretical framework of the nonlinear Gaussian noise model for hybrid fiber spans. We find a general expression for the nonlinear noise variance for the case of an arbitrary number of fiber types per span. Then, we elaborate on the accurate numerical evaluation of the integral for the nonlinear noise coefficient $\tilde{\gamma}$. The latter task consists in addressing four computational aspects: (1) Adopting a novel transformation of variables (other than using hyperbolic coordinates[7]) that changes the integrand to a more appropriate form for numerical quadrature; (2) Evaluating analytically the integral at its

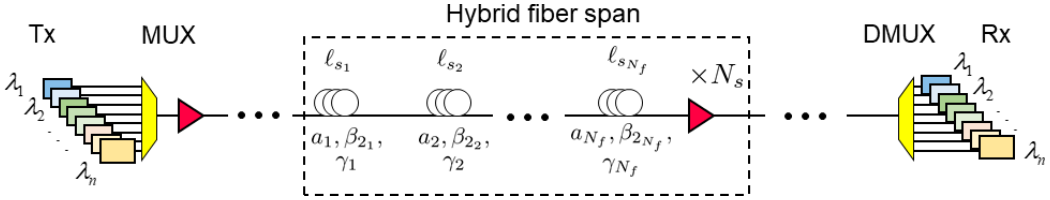

Fig. 1 Long-haul coherent optical communications system with hybrid fiber spans.

lower limit, where the integrand presents a singularity; (3) Dividing the interval of integration into panels of size π and approximating the integral in each panel by using various algorithms; and (4) Deriving an upper bound for the relative error due to the truncation of the range of integration to accelerate computation.

We apply the proposed model to coherent optical communications systems with fiber spans composed of quasi-single-mode fiber and single-mode fiber segments. The accuracy of the final analytical relationship for the nonlinear noise coefficient in long-haul coherent optical communications systems with hybrid fiber spans is checked using the split-step Fourier method and Monte Carlo simulation. It is shown to be adequate to within 0.1 dB for the determination of the optimal fiber segment lengths per span that maximize system performance.

2 Synopsis of the nonlinear Gaussian Noise (GN) model for hybrid fiber spans

2.1 System topology

Figure 1 depicts the block diagram of a representative long-haul coherent optical communication system with hybrid fiber spans. The transmission link of total length L is composed of a concatenation of N_s identical spans. Each span has length ℓ_s and comprises N_f fiber types. Each fiber type is characterized by its nonlinear fiber coefficient γ, which is a function of the effective mode area A_{eff} and the nonlinear index coefficient n_2; its Group Velocity Dispersion (GVD) parameter β_2 (or, equivalently, its chromatic dispersion parameter D); and its attenuation coefficient a. In what follows, the index k stands for the k-th fiber segment per span. For instance, the optical fiber lengths of the N_f segments are $\ell_{s_1}, \ell_{s_2}, \ldots, \ell_{s_{N_f}}$ and their effective mode areas are $A_{\text{eff}_1}, A_{\text{eff}_2}, \ldots, A_{\text{eff}_{N_f}}$, respectively. The optical fiber is followed by an optical amplifier of gain equal to the span loss $G = \exp\left(\sum_{i=1}^{N_f} a_i \ell_{s_i}\right)$ and noise figure F_A.

We consider WDM and Polarization Division Multiplexing (PDM) based on ideal Nyquist channel spectra. The latter are created using square-root raised cosine filters with zero roll-off factor at the transmitter and the receiver. Furthermore, we assume that the WDM signal is a superposition of an odd number N_{ch} wavelength channels with spacing $\Delta\nu = R_s$. We denote by P the total average launch power per channel (in both polarizations) and by R_s the symbol rate. We want to evaluate the performance of the center WDM channel at wavelength λ.

The performance of coherent optical systems without in-line chromatic dispersion compensation is related to the effective Optical Signal-to-Noise Ratio (OSNR_{eff}) at the receiver input. This quantity takes into account the Amplified Spontaneous Emission (ASE) noise, the MultiPath Interference (MPI) crosstalk (in the case of quasi-single-mode fibers), and the nonlinear distortion. All the above effects can be modeled as independent, zero-mean, and complex Gaussian noises with a good degree of accuracy. More specifically, the OSNR_{eff} at a resolution bandwidth $\Delta\nu_{\text{res}}$ can be well described by the analytical relationship[27]

$$\text{OSNR}_{\text{eff}} = \frac{P}{\tilde{a} + \tilde{\beta} P + \tilde{\gamma} P^3}, \tag{1}$$

where $\tilde{a}$ is the ASE noise variance, $\tilde{\beta} P$ is the crosstalk variance, and $\tilde{\gamma} P^3$ is the nonlinear noise variance. The coefficients $\tilde{a}$, $\tilde{\beta}$, and $\tilde{\gamma}$ depend on the fiber and system parameters[27].

2.2 Model overview

The purpose of this section is to derive an analytical formula for the nonlinear noise coefficient $\tilde{\gamma}$ in long-haul coherent optical communications systems with hybrid fiber spans.

To this end, we will extend the conventional nonlinear Gaussian noise model[6,7,9,16]—initially formulated for a single fiber type per span—then to multiple fiber types per span.

There are four steps used to calculate the variance of nonlinear noise in long-haul coherent optical communications systems with hybrid fiber spans:

(1) Solve the Manakov Eq. (2) by using regular perturbation theory in the frequency domain[28,29], assuming that the fiber attributes, i.e., the attenuation coefficient a, the GVD parameter β_2, and the nonlinear fiber coefficient γ, are piecewise constant functions of distance.

(2) Find an analytical expression for the first-order perturbation correction (Eq. (20)) to the unperturbed

wavefunction.

(3) Derive analytical expressions for the four-wave mixing efficiency for a single hybrid fiber span (Eqs. (27)–(29)) and multiple identical hybrid fiber spans (Eqs. (31)–(33)).

(4) Substitute the above expressions into the GNRF (see Ref. [6, Eq. (18)] or Ref. [9, Eq. (1)]) to obtain a double integral (Eq. (45)) for the nonlinear noise coefficient $\tilde{\gamma}$.

The final analytical expressions for calculating the nonlinear noise power spectral density in long-haul coherent optical communications systems with hybrid fiber spans are summarized in Table 1. We can make the following observations:

(1) As in the case of homogeneous fiber spans[7,9], the nonlinear noise coefficient $\tilde{\gamma}$ for hybrid fiber spans (Eq. (45)) depends on two factors: representing the four-wave mixing efficiency per span and the accumulation of four-wave mixing contributions from successive fiber spans (i.e., phased-array term).

(2) The four-wave mixing efficiency per span factor depends on the characteristics of the different fibers per span. It is expressed as a simple formula (Eq. (42)) that depends on two general parameters for each fiber: the complex nonlinear coefficient (Eq. (28)) and the normalized complex effective length (Eq. (29)).

(3) The coherent addition of the contributions of successive fiber spans to the total nonlinear noise is given by a phased-array factor (Eq. (41)). A major difference compared to the case of homogeneous fiber spans[7,9] is that, in the hybrid fiber span case, this factor depends on the average phase mismatch (Eq. (32)) of all optical fibers per span[24].

For computational convenience, the double integral can be converted into a single integral by using a transformation of integration variables. The final integral (see Eq. (59) in the main text) is an improper integral of the second kind (i.e., the integrand becomes infinite at the lower end of the integration interval). In addition, the integrand oscillates in the integration interval. The pseudocode for the numerical quadrature algorithm is shown below (see Algorithm 1). To accurately compute the integral (Eq. (59)) using numerical quadrature, it is necessary to analytically calculate the contribution in the vicinity of the singularity, then divide the remaining integration interval into π-subintervals, use a numerical quadrature method for each subinterval, and add up the results.

3 Manakov equation: Perturbation theory

Before presenting our analytical calculations, in this subsection, we review some terminology and notation used throughout this paper. A full list of symbols is given in the Appendix.

Table 1 Compendium of mathematical formulas summarizing the nonlinear Gaussian noise model for coherent optical communications systems with hybrid fiber spans. The numbers refer to the corresponding equations in the main text.

Main result (double integral form)			
Nonlinear noise coefficient			
$\tilde{\gamma} = \frac{64}{27}\frac{N_s \Delta\nu_{\mathrm{res}}}{R_s^3}\int_0^{\frac{B_0}{2}}\int_0^{\frac{B_0}{2}} \xi(f_1,f_2)\,\mathrm{d}f_1\mathrm{d}f_2$	(45)		
Integrand			
$\xi(f_1,f_2) \coloneqq \eta(f_1,f_2)\,\phi(f_1,f_2)$	(40)		
Auxiliary function			
FWM efficiency per span		Phased-array factor	
$\eta(f_1,f_2) \coloneqq \left\lvert\sum_{k=1}^{N_f} \hat{\gamma}_k(f_1,f_2)\,\hat{L}_{\mathrm{eff}_k}(f_1,f_2)\right\rvert^2$	(42)	$\phi(f_1,f_2) \coloneqq \frac{1}{N_s^2}\frac{\sin^2[N_s\Delta\beta(f_1,f_2)\ell_s/2)]}{\sin^2[\Delta\beta(f_1,f_2)\ell_s/2]}$	(41)
Complex nonlinear fiber coefficient		Average phase mismatch	
$\hat{\gamma}_k(f_1,f_2) \coloneqq \gamma_k \mathrm{e}^{-\sum_{m=1}^{k-1}\alpha_m(f_1,f_2)\ell_{s_m}}$	(28)	$\Delta\beta(f_1,f_2) \coloneqq \ell_s^{-1}\sum_{k=1}^{N_f}\Delta\beta_k(f_1,f_2)\ell_{s_k}$	(32)
Complex effective length			
$\hat{L}_{\mathrm{eff}_k}(f_1,f_2) \coloneqq \frac{1-\mathrm{e}^{-\alpha_k(f_1,f_2)\ell_{s_k}}}{\alpha_k(f_1,f_2)}$	(29)		

Algorithm 1 Pseudocode for the nonlinear noise coefficient.

Function $\tilde{\gamma}$

▷ $\tilde{\gamma}$ calculation

Input variables

Fiber parameters

a_k ▷ Attenuation coefficient
β_{2_k} ▷ GVD parameter
γ_k ▷ nonlinear coefficient
ℓ_{s_k} ▷ Segment length

System parameters

ℓ_s ▷ Span length
L_{tot} ▷ Link length
R_s ▷ Symbol rate
N_{ch} ▷ Number of WDM channels
N_f ▷ Number of fiber segments per span
F_A ▷ EDFA noise figure

Main code

▷ Lower end of the integral

$\text{sum} \leftarrow \kappa \left[\ln\left(\frac{\zeta_0}{\delta}\right) \int_0^{\delta} \xi(\zeta)\mathrm{d}\zeta + \delta\xi(0) \right]$

$N_{\text{int}} \leftarrow \lceil (\zeta_0 - \delta)/\pi \rceil$ ▷ Number of π-intervals

while $1 \leqslant n \leqslant N_{\text{int}}$ **do**

$\text{sum} \leftarrow \text{sum} + \kappa \int_{(n-1)\pi}^{n\pi} \ln\left(\frac{\zeta_0}{\zeta}\right) \xi(\zeta)\,\mathrm{d}\zeta$

end while

return sum ▷ Nonlinear coefficient $\tilde{\gamma}$

end function

Abbreviation: EDFA = Erbium-Doped Fiber Amplifier.

We represent the optical signal by a two-dimensional complex vector $\boldsymbol{y}(z,t)$, whose components are the complex envelopes[30] of the signals along the x, y States Of Polarization (SOPs). The vector components are functions of the position z inside the fiber and the time t.

We adopt the shorthand notation of Refs. [10, 14], for partial derivatives, where ∂_x denotes partial differentiation with respect to the independent variable x, ∂_x^2 denotes double partial differentiation with respect to x, and so forth. Similarly, using Euler's notation, the symbol D_x indicates a regular derivative with respect to x.

In the remainder of this section, we discuss the formal derivation of a general expression for the nonlinear noise coefficient $\tilde{\gamma}$ in Eq. (1). Our goal is to establish the connection among disparate formalisms in previous publications[22–25]. Portions of this formalism are taken from Refs. [7–9], with changes in notation.

Based on Agrawal's derivation[1] but using the engineering convention for the Fourier transform[30]*, the Manakov equation can be written as follows[31]:

$$\partial_z \boldsymbol{y}(z,t) + \frac{a(z)}{2}\boldsymbol{y}(z,t) - \frac{\iota\beta_2(z)}{2}\partial_t^2 \boldsymbol{y}(z,t) = -\iota\overline{\gamma}(z)\left\|\boldsymbol{y}(z,t)\right\|^2 \boldsymbol{y}(z,t), \tag{2}$$

where we neglected the third-order chromatic dispersion and the optical amplifier noise. Notice that $\overline{\gamma}(z) = 8\gamma(z)/9$[2].

The difference between the above form of the Manakov equation and the one used in the conventional nonlinear Gaussian noise model[7,9] is that we considered variable coefficients $a(z)$, $\beta_2(z)$, and $\gamma(z)$. Further down, we assume that $a(z)$, $\beta_2(z)$, and $\gamma(z)$, are piecewise constant functions of distance to express the fact that each optical fiber segment of a hybrid span has different characteristics.

3.1 Solution for harmonic waves

Based on the Manakov Eq. (2), we will study the nonlinear propagation of each spectral component of the launched optical signal through the optical fiber. Initially, we will assume that the signal generated by the optical transmitter is pseudorandom[7,9,12], i.e., periodic in time with period T_0. Due to the periodicity of the optical signal, its spectrum is composed of discrete spectral lines. Later in the paper, in Section 6, we will increase the signal period to infinity to deal with continuous signal spectra.

Since the launched optical signal is periodic, it can be expanded into exponential Fourier series

*For a time-domain signal $x(t)$ with spectrum $X(f)$, the direct Fourier transform is defined as $X(f) \coloneqq \int_{-\infty}^{\infty} x(t)\mathrm{e}^{-\iota 2\pi ft}\mathrm{d}t$ and the inverse Fourier transform is defined as $x(t) \coloneqq \int_{-\infty}^{\infty} X(f)\mathrm{e}^{\iota 2\pi ft}\mathrm{d}f$.

$$\boldsymbol{y}(z,t) = \sum_{n\in\mathbf{Z}} \boldsymbol{u}_n(z)\mathrm{e}^{\iota\omega_n t}, \tag{3}$$

where $f_0 = 1/T_0$ is the fundamental frequency, $f_n = nf_0$ are the Fourier harmonics, $\omega_n = 2\pi f_n$ are the corresponding angular frequencies, and $\boldsymbol{u}_n(z)$ are complex Fourier coefficients which are vector functions of position. Later on, we omit the limits of the infinite summation in the Fourier series in Eq. (3) to avoid clutter.

Substituting Eq. (3) for $\boldsymbol{y}(z,t)$ into the Manakov Eq. (2) gives

$$\sum_n \left[D_z\boldsymbol{u}_n(z) + \overline{a}_n(z)\,\boldsymbol{u}_n(z)\right]\mathrm{e}^{\iota\omega_n t} = -\iota\overline{\gamma}(z)\sum_{i,j,k}[\boldsymbol{u}_k^\dagger(z)\cdot\boldsymbol{u}_i(z)]\boldsymbol{u}_j(z)\mathrm{e}^{\iota(\omega_i+\omega_j-\omega_k)t}, \tag{4}$$

where a dagger † denotes the adjoint matrix and we set

$$\overline{a}_n(z) \coloneqq \frac{1}{2}\left[a(z) + \iota\beta_2(z)\,\omega_n^2\right]. \tag{5}$$

The Fourier coefficients of two equal functions are equal[32]. By equating the angular frequencies in the two sides of Eq. (4)

$$\omega_n = \omega_i + \omega_j - \omega_k, \tag{6}$$

as well as the corresponding Fourier coefficients, we obtain the following system of coupled, first-order, Ordinary Differential Equations (ODEs)

$$D_z\boldsymbol{u}_n(z) + \overline{a}_n(z)\,\boldsymbol{u}_n(z) = -\iota\overline{\gamma}(z)\sum_{(i,j,k)\in\Omega_n}[\boldsymbol{u}_k^\dagger(z)\cdot\boldsymbol{u}_i(z)]\boldsymbol{u}_j(z), \tag{7}$$

for $n\in\mathbf{Z}$, where Ω_n denotes the set of all index triplets for combinations of ω_i, ω_j, and ω_k that create nonlinear interference at angular frequency ω_n through four-wave mixing due to Kerr effect

$$\Omega_n \coloneqq \{(i,j,k)\in\mathbf{Z}^3 : \omega_n = \omega_i + \omega_j - \omega_k\}. \tag{8}$$

3.2 Perturbation theory

To formally apply perturbation theory to the problem at hand, we artificially insert a small parameter ε into the Right Hand Side (RHS) of Eq. (7)[29]

$$D_z\boldsymbol{u}_n(z) + \overline{a}_n(z)\,\boldsymbol{u}_n(z) = -\iota\varepsilon\overline{\gamma}(z)\sum_{(i,j,k)\in\Omega_n}[\boldsymbol{u}_k^\dagger(z).\boldsymbol{u}_i(z)]\boldsymbol{u}_j(z), \tag{9}$$

where we assumed that ε is small enough that the impact of nonlinear effects on the solution is a small perturbation. At the end of the calculation, we will again set $\varepsilon = 1$ to obtain an approximate analytical solution of Eq. (7). The accuracy of this solution will be determined by comparing the agreement among numerical and analytical results for the performance of various long-haul coherent optical communications systems.

We assume that the solution of Eq. (9) can be expressed in terms of power series of the small parameter ε[28,29]

$$\boldsymbol{u}_n(z) = \sum_{m=0}^{\infty}\boldsymbol{u}_{nm}(z)\varepsilon^m, \tag{10}$$

where the term $\boldsymbol{u}_{nm}(z)\varepsilon^m$ denotes the m-th order correction to the unperturbed solution $\boldsymbol{u}_{n0}(z)$.

By substituting Eq. (10) into the modified Manakov Eq. (9) and equating coefficients of like powers of ε, we obtain the following system of uncoupled, first-order, ODEs:

(1) Unperturbed ODE:

$$D_z\boldsymbol{u}_{n0}(z) + \overline{a}_n(z)\,\boldsymbol{u}_{n0}(z) = \boldsymbol{0}. \tag{11}$$

(2) ODE for the m-th order perturbation ($m \geqslant 1$):

$$D_z\boldsymbol{u}_{nm}(z) + \overline{a}_n(z)\,\boldsymbol{u}_{nm}(z) = -\iota\overline{\gamma}(z) \cdot \sum_{(i,j,k)\in\Omega_n}\sum_{(i',j',k')\in\Psi_m}[\boldsymbol{u}_{kk'}^\dagger(z)\cdot\boldsymbol{u}_{ii'}(z)]\boldsymbol{u}_{jj'}(z), \tag{12}$$

where Ψ_m denotes the set of non-negative integers i', j', and k'

$$\Psi_m \coloneqq \left\{(i',j',k')\in\mathbf{N}_0^3 : i'+j'+k'+1 = m\right\}, \tag{13}$$

where $\mathbf{N}_0$ is the set of natural numbers including zero.

In the following, we will retain only the first-order perturbation term

$$\boldsymbol{u}_n(z) \simeq \boldsymbol{u}_{n0}(z) + \varepsilon\boldsymbol{u}_{n1}(z). \tag{14}$$

The ODE for the first-order perturbation is given by Eq. (12) by setting $m = 1$

$$D_z\boldsymbol{u}_{n1}(z) + \overline{a}_n(z)\,\boldsymbol{u}_{n1}(z) = -\iota\overline{\gamma}(z)\sum_{(i,j,k)\in\Omega_n}[\boldsymbol{u}_{k0}^\dagger(z)\cdot\boldsymbol{u}_{i0}(z)]\boldsymbol{u}_{j0}(z). \tag{15}$$

The unperturbed ODE (Eq. (11)) can be solved by separation of variable

$$\boldsymbol{u}_{n0}(z) = \boldsymbol{c}_{n0}\mathrm{e}^{-\int_0^z\overline{a}_n(z')\mathrm{d}z'}, \tag{16}$$

where $\boldsymbol{c}_{n0}$ is the Fourier coefficient of the n-th spectral component at the fiber input.

Assume that the solution of Eq. (15) can be written in a form similar to Eq. (16)

$$\boldsymbol{u}_{n1}(z) = \boldsymbol{c}_{n1}(z)\mathrm{e}^{-\int_0^z\overline{a}_n(z')\mathrm{d}z'}, \tag{17}$$

where the complex coefficient $\boldsymbol{c}_{n1}(z)$ is a function of distance z to allow for nonlinear coupling introduced by the Kerr effect.

By substituting Eqs. (16) and (17) into Eq. (15), we obtain the simplified ODE

$$D_z\boldsymbol{c}_{n1}(z) = -\iota\overline{\gamma}(z) \sum_{(i,j,k)\in\Omega_n} [\boldsymbol{c}_{k0}^{\dagger}\cdot\boldsymbol{c}_{i0}]\boldsymbol{c}_{j0} \cdot \mathrm{e}^{-\int_0^z \overline{a}_{ijk}(z')\mathrm{d}z'}, \tag{18}$$

where we defined the complex attenuation coefficient

$$\overline{a}_{ijk}(z) := \overline{a}_i(z) + \overline{a}_j(z) + \overline{a}_k^*(z) - \overline{a}_n(z), \tag{19}$$

where star denotes the complex conjugate.

By integrating both sides of the above ODE over a single span length, we obtain

$$\boxed{\boldsymbol{c}_{n1}(\ell_s) = -\frac{8\iota}{9} \sum_{(i,j,k)\in\Omega_n} [\boldsymbol{c}_{k0}^{\dagger}\cdot\boldsymbol{c}_{i0}]\boldsymbol{c}_{j0} X_{ijk}(\ell_s)}, \tag{20}$$

where we defined the complex FWM efficiency $X_{ijk}(\ell_s)$

$$\boxed{X_{ijk}(\ell_s) := \int_0^{\ell_s} \gamma(z)\mathrm{e}^{-\int_0^z \overline{a}_{ijk}(z')\mathrm{d}z'}\mathrm{d}z}. \tag{21}$$

To derive Eq. (20), we assumed, as initial condition, that the complex amplitude of the nonlinear noise at the fiber input is zero, $\boldsymbol{c}_{n1} = \boldsymbol{0}$.

4 FWM efficiency for a single fiber span

Let's focus our attention on the complex constant $X_{ijk}(\ell_s)$ given by Eq. (21). By substituting Eqs. (5) and (6) into Eq. (19), the complex attenuation coefficient $\overline{a}_{ijk}$ can be rewritten as

$$\overline{a}_{ijk}(z) = a(z) + \iota\Delta\beta_{ijk}(z), \tag{22}$$

where $\Delta\beta_{ijk}(z)$ is the phase mismatch

$$\Delta\beta_{ijk}(z) := -\beta_2(z)(\omega_i - \omega_k)(\omega_j - \omega_k). \tag{23}$$

As a worst case scenario, we will calculate the nonlinear noise generated at the center of the WDM spectrum. Setting $n = 0$ in Eq. (6), we have

$$\omega_k = \omega_i + \omega_j. \tag{24}$$

We can then drop the subscript k from the notation and simplify the relationships of the complex attenuation coefficient and the phase mismatch

$$\overline{a}_{ij}(z) = a(z) + \iota\Delta\beta_{ij}(z), \tag{25a}$$

$$\Delta\beta_{ij}(z) = -\beta_2(z)\omega_i\omega_j. \tag{25b}$$

For hybrid fiber spans, the fiber attributes are constant within each segment. For the m-th fiber segment of the span, the above expressions are rewritten using slightly different notation for mathematical convenience

$$\alpha_m(i,j) := a_m + \iota\Delta\beta_m(i,j),$$
$$\Delta\beta_m(i,j) := -\beta_{2_m}\omega_i\omega_j, \tag{26}$$

where a_m is the (real) attenuation coefficient and β_{2_m} is the GVD parameter of the m-th fiber segment.

For the case of N_f fiber segments per span, we will show that the complex FWM efficiency for a single span is written as a sum

$$\boxed{X_{ij}(\ell_s) = \sum_{k=1}^{N_f} \hat{\gamma}_k(i,j)\hat{L}_{\mathrm{eff}_k}(i,j)}, \tag{27}$$

where the complex nonlinear fiber coefficients are defined as

$$\boxed{\hat{\gamma}_k(i,j) := \gamma_k \mathrm{e}^{-\sum_{m=1}^{k-1}\alpha_m(i,j)\ell_{s_m}}}, \tag{28}$$

and the complex effective lengths are defined as

$$\boxed{\hat{L}_{\mathrm{eff}_k}(i,j) := \frac{1-\mathrm{e}^{-\alpha_k(i,j)\ell_{s_k}}}{\alpha_k(i,j)}}. \tag{29}$$

Notice that Eq. (29) deviates from the traditional definition of the effective length[33]. The rationale behind our choice is that it allows us to write an easy-to-remember Eq. (27) for $X_{ij}(\ell_s)$.

Proof. Since the values of the fiber attributes a_k, β_{2_k}, and γ_k are different for different fiber segments but constant within each segment, we break up the integration interval in Eq. (21) into N_f subintervals of width ℓ_{s_k}. More specifically, we partition the z axis with a sequence of $N_f + 1$ points $z_0, \ldots, z_{N_f}$, where $z_0 = 0$ and $z_{N_f} = \ell_s$. The k-th fiber segment has endpoints z_{k-1} and z_k, and length $\ell_{s_k} = z_k - z_{k-1}$.

We shall integrate over different fiber segments separately and add the results

$$\begin{aligned} X_{ij}(\ell_s) &= \int_0^{\ell_s} \gamma(z)\,\mathrm{e}^{-\int_0^z \bar{a}_{ij}(z')\mathrm{d}z'}\mathrm{d}z \\ &= \sum_{k=1}^{N_f} \int_{z_{k-1}}^{z_k} \gamma(z)\mathrm{e}^{-\int_0^z \bar{a}_{ij}(z')\mathrm{d}z'}\mathrm{d}z. \end{aligned}$$

Since $\gamma(z)$ and $\exp\left[-\int_0^{z_{k-1}} \bar{a}_{ij}(z')\,\mathrm{d}z'\right]$ are constant within the subinterval $[z_{k-1}, z_k]$, they can be factored out of the integral

$$X_{ij}(\ell_s) = \sum_{k=1}^{N_f} \gamma_k \mathrm{e}^{-\int_0^{z_{k-1}} \bar{a}_{ij}(z')\mathrm{d}z'} \cdot \int_{z_{k-1}}^{z_k} \mathrm{e}^{-\int_{z_{k-1}}^{z} \bar{a}_{ij}(z')\mathrm{d}z'}\mathrm{d}z.$$

Performing the integration in the exponents of the last expression yields

$$X_{ij}(\ell_s) = \sum_{k=1}^{N_f} \gamma_k \mathrm{e}^{-\sum_{m=1}^{k-1} \int_{z_{m-1}}^{z_m} \bar{a}_{ij}(z')\mathrm{d}z'} \cdot \int_{z_{k-1}}^{z_k} \mathrm{e}^{-\bar{a}_{ij}(z)(z-z_{k-1})}\mathrm{d}z.$$

Since $\bar{a}_{ij}(z')$ is constant within each subinterval $[z_{k-1}, z_k]$ and using a change of integration variables for the latter integral, we obtain

$$X_{ij}(\ell_s) = \sum_{k=1}^{N_f} \gamma_k \mathrm{e}^{-\sum_{m=1}^{k-1} \alpha_m(i,j)\ell_{s_m}} \cdot \int_0^{\ell_{s_k}} \mathrm{e}^{-\alpha_k(i,j)z}\mathrm{d}z.$$

Using the definitions for the complex nonlinear fiber coefficients (Eq. (28)) and the complex effective lengths (Eq. (29)), it is straightforward to show that

$$X_{ij}(\ell_s) = \sum_{k=1}^{N_f} \gamma_k \mathrm{e}^{-\sum_{m=1}^{k-1} \alpha_m(i,j)\ell_{s_m}} \frac{1-\mathrm{e}^{-\alpha_k(i,j)\ell_{s_k}}}{\alpha_k(i,j)} = \sum_{k=1}^{N_f} \hat{\gamma}_k(i,j)\hat{L}_{\mathrm{eff}_k}(i,j). \quad (30)$$

■

5 FWM efficiency for multiple identical hybrid fiber spans

For N_s identical spans of length ℓ_s with N_f fiber types per span and lumped optical amplifiers between successive spans to compensate for fiber attenuation, we will show that the complex FWM efficiency is given by

$$\boxed{X_{ij}(N_s\ell_s) = X_{ij}(\ell_s)\frac{\sin[N_s\Delta\beta(i,j)\ell_s/2]}{\sin[\Delta\beta(i,j)\ell_s/2]} \cdot \mathrm{e}^{-\iota(N_s-1)\Delta\beta(i,j)\ell_s/2}}, \quad (31)$$

where $\Delta\beta$ is the average propagation constant mismatch

$$\boxed{\Delta\beta(i,j) := \ell_s^{-1}\sum_{k=1}^{N_f}\Delta\beta_k(i,j)\ell_{s_k}}, \quad (32)$$

or, equivalently, β_2 is the average GVD parameter

$$\boxed{\beta_2 := \ell_s^{-1}\sum_{k=1}^{N_f}\beta_{2_k}\ell_{s_k}}. \quad (33)$$

Proof. Consider a link composed of N_s identical spans of length ℓ_s. The fiber attributes $a(z)$, $\beta_2(z)$, and $\gamma(z)$ are periodic functions with fundamental period ℓ_s. Therefore, we can write

$$a(z) = a(z - m\ell_s), \quad (34a)$$

$$\beta_2(z) = \beta_2(z - m\ell_s), \quad (34b)$$

$$\gamma(z) = \gamma(z - m\ell_s), \quad (34c)$$

for $m \in \mathbf{Z}$, $z \in [0, N_s\ell_s]$, and $z - m\ell_s \in [0, \ell_s]$.

It follows that the complex attenuation coefficients $\bar{a}_{ij}(z)$ are also periodic functions with period ℓ_s. Thus, we can write

$$\bar{a}_{ij}(z) = \bar{a}_{ij}(z - m\ell_s), \quad (35)$$

for $m \in \mathbf{Z}$ and z as above.

To calculate $X_{ij}(N_s\ell_s)$, we start from Eq. (21), break up the integration interval into subintervals of width ℓ_s, and use the periodicity of Eqs. (34a)–(34c) and (35) to obtain

$$X_{ij}(N_s\ell_s) = \int_0^{N_s\ell_s} \gamma(z)\,\mathrm{e}^{-\int_0^z \bar{a}_{ij}(z')\mathrm{d}z'}\mathrm{d}z = \sum_{m=0}^{N_s-1}\left\{\int_{m\ell_s}^{(m+1)\ell_s} \gamma(z-m\ell_s)\mathrm{e}^{-\int_{m\ell_s}^z \bar{a}_{ij}(z'-m\ell_s)\mathrm{d}z'}\mathrm{d}z\right\} \cdot \mathrm{e}^{-\int_0^{m\ell_s}\bar{a}_{ij}(z')\mathrm{d}z'}.$$

By changing the integration variables for the integrals in the curly brackets in Eq. (35), we obtain

$$X_{ij}(N_s\ell_s) = \left\{\int_0^{\ell_s}\gamma(z)\mathrm{e}^{-\int_0^z \bar{a}_{ij}(z')\mathrm{d}z'}\mathrm{d}z\right\}\sum_{m=0}^{N_s-1}\mathrm{e}^{-\int_0^{m\ell_s}\bar{a}_{ij}(z')\mathrm{d}z'} = X_{ij}(\ell_s)\sum_{m=0}^{N_s-1}\mathrm{e}^{-\sum_{q=0}^{m-1}\int_{q\ell_s}^{(q+1)\ell_s}\bar{a}_{ij}(z'-q\ell_s)\mathrm{d}z'}.$$

By performing a change of integration variables for the integral in the exponent, we obtain

$$X_{ij}(N_s\ell_s) = X_{ij}(\ell_s)\sum_{m=0}^{N_s-1}\mathrm{e}^{-m\int_0^{\ell_s}\bar{a}_{ij}(z')\mathrm{d}z'}. \quad (36)$$

Due to periodic amplification at the end of each span, we discard the real part of $\int_0^{\ell_s}\bar{a}_{ij}(z')\mathrm{d}z'$ and replace the latter integral with $\iota\int_0^{\ell_s}\Delta\beta_{ij}(z')\mathrm{d}z'$.

Using the definition of Eq. (32) yields

$$X_{ij}(N_s\ell_s) = X_{ij}(\ell_s)\sum_{m=0}^{N_s-1}\mathrm{e}^{-\iota m\Delta\beta(i,j)\ell_s}. \quad (37)$$

Finally, by summing the geometric series in Eq. (37), we get

$$X_{ij}\left(N_s\ell_s\right) = X_{ij}\left(\ell_s\right)\frac{1-\mathrm{e}^{-\iota N_s\Delta\beta(i,j)\ell_s}}{1-\mathrm{e}^{-\iota\Delta\beta(i,j)\ell_s}} = X_{ij}\left(\ell_s\right)\frac{\sin\left[N_s\Delta\beta(i,j)\ell_s/2\right]}{\sin\left[\Delta\beta(i,j)\ell_s/2\right]} \cdot \mathrm{e}^{-\iota(N_s-1)\Delta\beta(i,j)\ell_s/2}. \quad (38)$$

■

6 General formula for the nonlinear noise variance for hybrid fiber spans

In this subsection, a passage is made from discrete to continuous signal spectra when the period of the transmitted signal $T_0 \to \infty$. In the following integrals, we substitute the dummy variables f_1 and f_2 for the frequency components f_i and f_j, and abandon the indices i and j, used so far to keep track of the frequencies in the discrete setting.

We consider an aperiodic WDM PDM signal that results from the superposition of N_{ch} wavelength channels modulated at symbol rate R_s. Substituting our main result Eq. (31) into the nonlinear GNRF[6, Eq. (18)], the nonlinear noise psd $G_{\mathrm{NLI}}\left(f\right)$ can be written as

$$\boxed{G_{\mathrm{NLI}}\left(f\right) \cong \frac{16}{27}N_s^2\int_{-\infty}^{\infty}\int_{-\infty}^{\infty}G(f_1)G(f_2) \cdot G(f_1+f_2-f)\xi\left(f_1-f, f_2-f\right)\mathrm{d}f_1\mathrm{d}f_2}, \quad (39)$$

where $G(f)$ is the psd of the transmitted PDM WDM signal and the integrand equals as follows:

$$\boxed{\xi\left(f_1, f_2\right) \coloneqq \phi\left(f_1, f_2\right)\eta\left(f_1, f_2\right)}. \quad (40)$$

The first factor in Eq. (40) is the normalized phased-array term, defined as

$$\boxed{\phi\left(f_1, f_2\right) \coloneqq \frac{1}{N_s^2}\frac{\sin^2\left[N_s\Delta\beta\left(f_1, f_2\right)\ell_s/2\right)]}{\sin^2\left[\Delta\beta\left(f_1, f_2\right)\ell_s/2\right]}}, \quad (41)$$

where $\Delta\beta$ is the average phase mismatch in Eq. (32).

The second factor in Eq. (40) is the four-wave mixing efficiency, defined as

$$\boxed{\eta\left(f_1, f_2\right) \coloneqq \left|\sum_{k=1}^{N_f}\hat{\gamma}_k\left(f_1, f_2\right)\hat{L}_{\mathrm{eff}_k}\left(f_1, f_2\right)\right|^2}, \quad (42)$$

which is the continuous counterpart of $|X_{ij}\left(\ell_s\right)|^2$ (see Eq. (27)).

7 Special case: Ideal Nyquist WDM spectra with zero roll-off factor

In the remainder of the paper, we focus on ideal Nyquist WDM spectra with zero roll-off factor. Furthermore, we assume that the WDM signal is a superposition of an odd number N_{ch} wavelength channels with spacing $\Delta\nu = R_s$. The optical bandwidth of the WDM signal is

$$B_0 = N_{\mathrm{ch}}R_s\,. \quad (43)$$

Approximating the hexagonal integration region[7,9], resulting from Eq. (39) by a square, the nonlinear noise coefficient for the central WDM wavelength channel, measured in a resolution bandwidth $\Delta\nu_{\mathrm{res}}$, is given by the double integral

$$\tilde{\gamma} \simeq \frac{16}{27}\frac{N_s^2\Delta\nu_{\mathrm{res}}}{R_s^3}\int_{-B_0/2}^{B_0/2}\int_{-B_0/2}^{B_0/2}\xi\left(f_1, f_2\right)\mathrm{d}f_1\mathrm{d}f_2\,. \quad (44)$$

7.1 Single-integral formulation

We shall use a transformation of variables and iterated integration to convert Eq. (44) into a single integral.

To begin, since $\xi(f_1, f_2)$ is an even function of f_1 and f_2, we can reduce the region of integration to the upper right quadrant of the coordinate plane

$$\boxed{\tilde{\gamma} = \frac{64}{27}\frac{N_s^2\Delta\nu_{\mathrm{res}}}{R_s^3}\int_0^{B_0/2}\int_0^{B_0/2}\xi\left(f_1, f_2\right)\mathrm{d}f_1\mathrm{d}f_2}\,. \quad (45)$$

The integrand $\xi\left(f_1, f_2\right)$ depends only on the product of the integration variables $f_1 f_2$, so it is beneficial to define a new integration variable ζ that is directly proportional to $f_1 f_2$

$$\zeta \coloneqq \frac{\Delta\beta\ell_s}{2} = \frac{f_1 f_2}{2f_\phi^2}\,, \quad (46)$$

where f_ϕ is the average phased-array bandwidth[3] defined as

$$f_\phi^{-1} \coloneqq 2\pi\sqrt{|\beta_2|\,\ell_s}\,. \quad (47)$$

Then, we change the integration variables from f_1 and f_2 to f_1, ζ. By holding f_1 fixed and differentiating with respect to f_2, we obtain $\mathrm{d}\zeta = f_1\mathrm{d}f_2/(2f_\phi^2)$, or, equivalently, $\mathrm{d}f_2 = (2f_\phi^2/f_1)\mathrm{d}\zeta$. Since the upper limit of the integral in f_2 is $f_2 = B_0/2$, the upper limit of the integral in ζ becomes $\zeta = f_1 B_0/(4f_\phi^2)$.

With these substitutions, we obtain

$$\tilde{\gamma} = \frac{128}{27}\frac{N_s^2\Delta\nu_{\mathrm{res}}}{R_s^3}f_\phi^2\int_0^{\frac{B_0}{2}}\left[\int_0^{\frac{f_1 B_0}{4f_\phi^2}}\xi\left(\zeta\right)\mathrm{d}\zeta\right]\frac{\mathrm{d}f_1}{f_1}\,. \quad (48)$$

Finally, we change the order of integration to transform the double integral into a single integral. By changing the integration order, the range of f_1 becomes $[(4f_\phi^2\zeta)/B_0, B_0/2]$. Now ζ is the integration variable of the outer integral. Its limits correspond to the total range of ζ over the integration region $[0, B_0^2/(8f_\phi^2)]$. Hence,

$$\tilde{\gamma} = \frac{128}{27}\frac{N_s^2 \Delta\nu_{\text{res}}}{R_s^3} f_\phi^2 \int_0^{\frac{B_0^2}{8f_\phi^2}} \left[\int_{4f_\phi^2\zeta/B_0}^{B_0/2} \frac{\mathrm{d}f_1}{f_1} \right] \xi(\zeta)\,\mathrm{d}\zeta\,. \tag{49}$$

The inner integral is elementary and can be calculated in closed-form. Therefore, the double integral can be transformed into a single-integral

$$\tilde{\gamma} = \frac{128}{27}\frac{\Delta\nu_{\text{res}}}{R_s^3} N_s^2 f_\phi^2 \int_0^{B_0^2/(8f_\phi^2)} \ln\left(\frac{B_0^2}{8\zeta f_\phi^2}\right) \xi(\zeta)\,\mathrm{d}\zeta\,. \tag{50}$$

The latter integral must be computed using numerical quadrature.

7.2 Useful auxiliary quantities

In this subsection, we shall define some useful auxiliary quantities that will enable us to rewrite the integrand of Eq. (50) in a more appropriate form for computation.

Notice that $\hat{\gamma}_k$ and $\hat{L}_{\text{eff}_k}$ are given by Eqs. (28) and (29), respectively, which depends on the products $\alpha_k \ell_{s_k}$. We can substitute these products by new complex coefficients $x_k \coloneqq \alpha_k \ell_{s_k}$.

We can rewrite $\hat{\gamma}_k$ as

$$\hat{\gamma}_k(\zeta) = \gamma_k \mathrm{e}^{-\sum_{m=1}^{k-1} x_m(\zeta)}\,, \tag{51}$$

and $\hat{L}_{\text{eff}_k}$ as

$$\hat{L}_{\text{eff}_k}(\zeta) = \ell_{s_k} \frac{1-\mathrm{e}^{-x_k(\zeta)}}{x_k(\zeta)}\,, \tag{52}$$

where, as mentioned above, we defined the normalized power complex attenuation coefficients $x_k(\zeta)$ as

$$x_k(\zeta) \coloneqq \alpha_k(\zeta)\,\ell_{s_k} = 2[\nu_k + \imath\zeta_k(\zeta)]\,, \tag{53}$$

where ν_k stands for the normalized electric field attenuation coefficient,

$$\nu_k \coloneqq \frac{a_k \ell_{s_k}}{2}\,, \tag{54}$$

and $\zeta_k(\zeta)$ for the normalized electric field phase shift,

$$\zeta_k(\zeta) \coloneqq \frac{\Delta\beta_k \ell_{s_k}}{2} = \frac{f_1 f_2}{2f_{\phi_k}^2} = \frac{f_\phi^2}{f_{\phi_k}^2}\zeta\,. \tag{55}$$

Similar to Eq. (47), f_{ϕ_k} in Eq. (55) denotes the phased-array bandwidth for each fiber segment

$$f_{\phi_k}^{-1} \coloneqq 2\pi\sqrt{|\beta_{2k}|\,\ell_{s_k}}\,. \tag{56}$$

To further simplify the notation in Eq. (55), we can define the multiplicative coefficients

$$\overline{\lambda}_k \coloneqq \frac{f_\phi^2}{f_{\phi_k}^2}\,, \tag{57}$$

so that the arguments $\zeta_k(\zeta)$ can be rewritten in compact form as a function of $\overline{\lambda}_k$ and ζ

$$\zeta_k(\zeta) \coloneqq \overline{\lambda}_k \zeta\,. \tag{58}$$

7.3 Final expressions

After these definitions, the formalism for calculating the nonlinear noise coefficient $\tilde{\gamma}$ can be rewritten in compact form.

From Eq. (50), the nonlinear noise coefficient, measured in a resolution bandwidth $\Delta\nu_{\text{res}} = R_s$, is expressed as a single definite integral

$$\boxed{\tilde{\gamma} = \kappa \int_0^{\zeta_0} \ln\left(\frac{\zeta_0}{\zeta}\right) \xi(\zeta)\,\mathrm{d}\zeta}\,, \tag{59}$$

where we defined

$$\kappa \coloneqq \frac{128}{27}\frac{f_\phi^2}{R_s^2} N_s^2\,, \tag{60}$$

$$\zeta_0 \coloneqq \frac{B_0^2}{8f_\phi^2}\,. \tag{61}$$

The efficiency function $\xi(\zeta)$ is written as a product

$$\boxed{\xi(\zeta) = \phi(\zeta)\,\eta(\zeta)}\,, \tag{62}$$

of the normalized phased-array term

$$\boxed{\phi(\zeta) = \frac{1}{N_s^2}\frac{\sin^2(N_s\zeta)}{\sin^2(\zeta)}}\,, \tag{63}$$

and the four-wave mixing efficiency

$$\boxed{\eta(\zeta) = \left|\sum_{k=1}^{N_f} \hat{\gamma}_k(\zeta)\,\hat{L}_{\text{eff}_k}(\zeta)\right|^2}\,. \tag{64}$$

8 Numerical method

8.1 Improper integral

We want to numerically evaluate the integral of Eq. (59), which we rewrite below without the coefficient κ

$$I = \int_0^{\zeta_0} \ln\left(\frac{\zeta_0}{\zeta}\right) \xi(\zeta)\mathrm{d}\zeta\,. \tag{65}$$

This is an improper integral of the second kind since the integrand has a singularity at zero, $\lim_{\zeta\to 0}(\zeta_0/\zeta) = \infty$.

In order to evaluate I, we split the integration interval into two sub-intervals

$$I = \int_0^{\delta} \ln\left(\frac{\zeta_0}{\zeta}\right) \xi(\zeta)\mathrm{d}\zeta + \int_\delta^{\zeta_0} \ln\left(\frac{\zeta_0}{\zeta}\right) \xi(\zeta)\mathrm{d}\zeta\,, \tag{66}$$

where δ is in the vicinity of $\zeta = 0$.

Some insight into the behavior of the integrand of Eq. (65) can be obtained from Fig. 2. As indicated by the red line, $g(\zeta) = \ln(\zeta_0/\zeta)\,\xi(\zeta)$ is oscillatory. The oscillation is mainly due to the phased-array factor

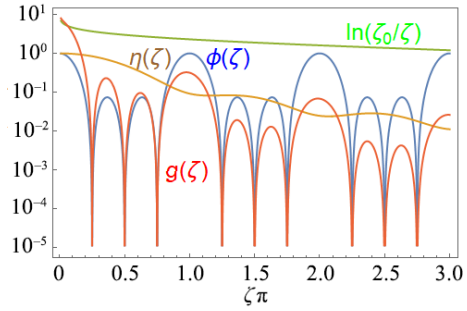

Fig. 2 Sketches of $\ln(\zeta_0/\zeta)$ (in green), $\phi(\zeta)$ (in blue), the normalized $\eta(\zeta) \leftarrow \eta(\zeta)/\eta(0)$ (in brown), and their product $g(\zeta) = \ln(\zeta_0/\zeta)\phi(\zeta)\eta(\zeta)/\eta(0)$ (in red). Conditions (for illustration purposes only): $N_s = 4$, $\nu = 1$, $\zeta_0 = 10\pi$, one fiber type per span.

$\phi(\zeta)$ (in blue), which is a periodic function with period π. Principal maxima of unit height occur at integer multiples of π. Between consecutive principal maxima (i.e., over a range of π) there are $N_s - 1$ minima at multiples of π/N_s and $N_s - 2$ subsidiary maxima approximately midway between successive minima. Thus, for a large number of spans N_s, the multiple-slit interference term $\phi(\zeta)$ rapidly varies over the integration region.

For the first integral in Eq. (66), we can write

$$\int_0^{\delta} \ln\left(\frac{\zeta_0}{\zeta}\right)\xi(\zeta)\mathrm{d}\zeta = \ln\left(\frac{\zeta_0}{\delta}\right)\int_0^{\delta}\xi(\zeta)\mathrm{d}\zeta + \int_0^{\delta}\ln\left(\frac{\delta}{\zeta}\right)\xi(\zeta)\mathrm{d}\zeta. \quad (67)$$

For the second integral in Eq. (67), taking the Taylor expansion of $\xi(\zeta)$ and integrating by parts, we obtain the following expression:

$$\int_0^{\delta}\ln\left(\frac{\delta}{\zeta}\right)\xi(\zeta)\mathrm{d}\zeta = \sum_{k=0}^{\infty}\frac{\delta^{k+1}}{k!(k+1)^2}D_{\zeta}^{k}\xi(0). \quad (68)$$

An alternative expression is given by Eq. (77) in Section 8.2.

Since $\eta(\zeta)$ (in brown in Fig. 2) is a slowly varying function of ζ, in a small interval $[0, \delta]$, we can use the approximation $\xi(\zeta) \cong \eta(0)\phi(\zeta)$ in Eq. (68). From L'Hôpital's rule, $\phi(0) = 1$. The odd derivatives of $\phi(\zeta)$ are zero. The first few even derivatives $\partial_{\zeta}^{2k}\phi(0)$, for $k \in \mathbf{N}$, can be evaluated analytically,

$$\partial_{\zeta}^{2}\phi(0) = -\frac{2}{3}\left(N_s^2 - 1\right), \quad (69)$$

$$\partial_{\zeta}^{4}\phi(0) = \frac{8}{15}\left(2N_s^4 - 5N_s^2 + 3\right). \quad (70)$$

For sufficiently small δ, keeping only the zeroth-order term of the sum in the RHS of Eq. (68) is appropriate

$$\int_0^{\delta}\ln\left(\frac{\zeta_0}{\zeta}\right)\xi(\zeta)\mathrm{d}\zeta \cong \ln\left(\frac{\zeta_0}{\delta}\right)\int_0^{\delta}\xi(\zeta)\mathrm{d}\zeta + \delta\xi(0). \quad (71)$$

We can evaluate δ in Eq. (71) by imposing the condition that the zeroth-order term of the Taylor series in Eq. (68) should be much larger than the subsequent terms so that we can truncate the Taylor series to the zeroth-order term. Consequently, δ should satisfy the following inequality:

$$\frac{\delta^3}{2!3^2}|\partial_{\zeta}^{2}\xi(0)| \ll \delta\xi(0), \quad (72)$$

which yields

$$\delta \ll \sqrt{\frac{2!3^2}{|\partial_{\zeta}^{2}\phi(0)|}} \overset{\text{Eq.(69)}}{=} \sqrt{\frac{3^3}{\left(N_s^2-1\right)}} \simeq \frac{3\sqrt{3}}{N_s}, \quad (73)$$

for $N_s \gg 1$.

Then, the two remaining integrals

$$\int_{\delta}^{\zeta_0}\ln\left(\frac{\zeta_0}{\zeta}\right)\xi(\zeta)\mathrm{d}\zeta, \quad (74)$$

and

$$\int_0^{\delta}\xi(\zeta)\mathrm{d}\zeta. \quad (75)$$

in Eqs. (66) and (67), respectively, can be calculated numerically.

There are several numerical quadrature methods for highly oscillatory integrals[34]. A rudimentary technique to uniformly sample the oscillatory integrand is Simpson's quadrature[35]. The integration interval can be subdivided into subintervals of width π/N_s. We sample each subinterval N_n times. Therefore, the distance between adjacent nodes is $\Delta = \pi/(N_s N_n)$.

We have approximately $N_{\text{int}} = \lceil \zeta_0/\pi \rceil$ periods of $\phi(\zeta)$ in the interval $[0, \zeta_0]$. Then, we have $N_{\text{int}} N_s N_n$ nodes in the interval $[0, N_{\text{int}}\pi]$. Summing slices along the ζ axis can become cumbersome, since Eqs. (43) and (61) give

$$N_{\text{int}} = \left\lceil \frac{N_{ch}^2 R_s^2 |\beta_2| \ell_s}{2} \right\rceil, \quad (76)$$

so the number of periods of the multiple-slit interference term $\phi(\zeta)$ in the integration interval increases proportionally to the span length ℓ_s and quadratically with the number of WDM channels N_{ch} and the symbol rate R_s.

Alternatively, the integral can be numerically evaluated using a commercial software tool like Mathematica[36]. For instance, the highly-oscillatory

integral Eq. (65) can be accurately computed by partitioning the integration interval into π subintervals, using the function NIntegrate in Mathematica, and adding up the results.

8.2 A more rigorous treatment of the integral value in the vicinity of singularity

We will show that the part of the integral $I(0,\delta)$ contributed by a small interval $(0,\delta)$ in the neighborhood of zero is given by

$$\begin{aligned} I(0,\delta) &= \int_0^{\delta} \ln\left(\frac{\zeta_0}{\zeta}\right)\xi(\zeta)\mathrm{d}\zeta \\ &\simeq \frac{\eta(0)}{N_s}\ln\left(\frac{\zeta_0}{\delta}\right)\left[\delta + \sum_{j=1}^{N_s-1}\left(1-\frac{j}{N_s}\right)\sin(2j\delta)\right] \\ &+ \frac{\eta(0)}{N_s}\left[\delta + \sum_{j=1}^{N_s-1}\left(1-\frac{j}{N_s}\right)\mathrm{Si}(2j\delta)\right], \end{aligned} \tag{77}$$

where $\mathrm{Si}(x)$ denotes the sine integral

$$\mathrm{Si}(x) := \int_0^x \frac{\sin(t)}{t}\,\mathrm{d}t.$$

The estimate of Eq. (77) is derived by assuming that δ is sufficiently small, so that $\eta(\zeta) \simeq \eta(0)$.

Proof. We notice that the phased-array term, when multiplied by N_s, coincides with the Fejér kernel[37]

$$N_s\phi(\zeta) = \frac{1}{N_s}\frac{\sin^2(N_s\zeta)}{\sin^2(\zeta)} = \sum_{j=-N_s+1}^{N_s-1}\left(1-\frac{|j|}{N_s}\right)\mathrm{e}^{2\imath j\zeta}, \tag{78}$$

which arises in the Cesàro summation of the Fourier series of π periodic functions. In particular, it is π-periodic, non-negative, and with period average

$$\frac{1}{\pi}\int_0^{\pi} N_s\phi(\zeta)\,\mathrm{d}\zeta = 1. \tag{79}$$

First, we rewrite the sum of Eq. (78) in real form

$$N_s\phi(\zeta) = 1 + 2\sum_{j=1}^{N_s-1}\left(1-\frac{j}{N_s}\right)\cos(2j\zeta). \tag{80}$$

Then, it is straightforward to show that

$$\int_0^x N_s\phi(\zeta)\mathrm{d}\zeta = x + \sum_{j=1}^{N_s-1}\left(\frac{1}{j}-\frac{1}{N_s}\right)\sin(2jx). \tag{81}$$

Next, we compute the following auxiliary integral:

$$K_{N_s}(\delta) := \int_0^{\delta}\ln(\delta/\zeta)N_s\phi(\zeta)\mathrm{d}\zeta. \tag{82}$$

Notice that $K_{N_s}(\delta)$ can be rewritten as a double integral

$$K_{N_s}(\delta) = \int_0^{\delta}\left[\int_{\zeta}^{\delta}\frac{1}{s}\mathrm{d}s\right]N_s\phi(\zeta)\mathrm{d}\zeta.$$

By switching the order of integration, we obtain

$$\begin{aligned} K_{N_s}(\delta) &= \int_0^{\delta}\frac{1}{s}\left[\int_0^{s}N_s\phi(\zeta)\mathrm{d}\zeta\right]\mathrm{d}s \\ &= \int_0^{\delta}\frac{1}{s}\left[s + \sum_{j=1}^{N_s-1}\left(\frac{1}{j}-\frac{1}{N_s}\right)\sin(2js)\right]\mathrm{d}s \\ &= \delta + \sum_{j=1}^{N_s-1}\left(\frac{1}{j}-\frac{1}{N_s}\right)\int_0^{\delta}\frac{\sin(2js)}{s}\mathrm{d}s \\ &= \delta + \sum_{j=1}^{N_s-1}\left(\frac{1}{j}-\frac{1}{N_s}\right)\int_0^{2j\delta}\frac{\sin(t)}{t}\mathrm{d}t \\ &= \delta + \sum_{j=1}^{N_s-1}\left(\frac{1}{j}-\frac{1}{N_s}\right)\mathrm{Si}(2j\delta). \end{aligned} \tag{83}$$

We can write

$$\begin{aligned} I(0,\delta) &= \int_0^{\delta}\ln\left(\frac{\zeta_0}{\zeta}\right)\xi(\zeta)\mathrm{d}\zeta \\ &= \frac{1}{N_s}\int_0^{\delta}\ln\left(\frac{\zeta_0}{\zeta}\right)N_s\phi(\zeta)\eta(\zeta)\mathrm{d}\zeta \\ &\simeq \frac{\eta(0)}{N_s}\left[\ln\left(\frac{\zeta_0}{\delta}\right)\int_0^{\delta}N_s\phi(\zeta)\mathrm{d}\zeta \right. \\ &\left. + \int_0^{\delta}\ln\left(\frac{\delta}{\zeta}\right)N_s\phi(\zeta)\mathrm{d}\zeta\right]. \end{aligned} \tag{84}$$

Substituting Eqs. (81) and (83) into Eq. (84), we arrive at Eq. (77). ■

8.3 Truncation error

In this section, we estimate the tail contribution to the integral I in Eq. (65), as given by

$$I(\mu,\zeta_0) := \int_{\mu}^{\zeta_0}\ln\left(\frac{\zeta_0}{\zeta}\right)\xi(\zeta)\mathrm{d}\zeta. \tag{85}$$

To simplify formulas, we take the ζ cutoff value $\mu \in (0,\zeta_0)$ of the form $\mu = (M+1)\pi$, where M is a natural number. When considering large ζ_0, little is lost in assuming that ζ_0 is also a multiple of π, $\zeta_0 = (N+1)\pi$. Our goal is to prove the following rigorous upper bound:

$$N_s I(\mu,\zeta_0) \leqslant \Gamma^2\frac{1}{\sigma}\mathrm{arccot}\left(\frac{M\pi}{\sigma}\right)\ln\left(\frac{\zeta_0}{M\pi}\right) \tag{86a}$$

$$\leqslant \Gamma^2\frac{1}{M\pi}\ln\left(\frac{\zeta_0}{M\pi}\right), \tag{86b}$$

where Γ, defined in Eq. (93) in the following, captures the non-linearity and σ, defined in Eq. (91), is the

minimal adjusted attenuation. The second inequality (based on $\operatorname{arccot}(x) \leqslant 1/x$ for $x > 0$) reflects the $1/M$ asymptotics for large M. The upshot is that, when ζ_0 is large and the oscillatory integrand in I becomes problematic, I can be typically approximated to be within a few percent by its truncated version

$$I(0,\mu) := \int_0^{\mu} \ln\left(\frac{\zeta_0}{\zeta}\right) \xi(\zeta) \mathrm{d}\zeta \,, \tag{87}$$

with a rigorous relative error ϵ_r bound

$$\epsilon_r \leqslant \frac{\Gamma^2}{M\pi N_s I(0,\mu)} \ln\left(\frac{\zeta_0}{M\pi}\right). \tag{88}$$

Proof. We derive Eq. (86a) now. Substituting in Eq. (64) the definitions of the complex nonlinear coefficients $\hat{\gamma}_k(\zeta)$ and complex effective lengths $\hat{L}_{\mathrm{eff}_k}(\zeta)$ in Eq. (64), given by Eqs. (51) and (52), yields a more detailed formula for the FWM efficiency

$$\eta(\zeta) = \left| \sum_{k=1}^{N_f} \gamma_k \frac{\ell_{s_k}}{\lambda_k} \mathrm{e}^{-\sum_{m=1}^{k-1} 2\lambda_m(\sigma_m+\iota\zeta)} \frac{1-\mathrm{e}^{-2\lambda_k(\sigma_k+\iota\zeta)}}{2(\sigma_k+\iota\zeta)} \right|^2, \tag{89}$$

to best capture the dependence on ζ, we introduced normalized, chromatic dispersion-adjusted, and real attenuation coefficients for each fiber type

$$\sigma_k := \frac{\nu_k}{\lambda_k} = \frac{1}{2}\frac{|\beta_2|}{|\beta_{2_k}|} a_k \ell_s \,. \tag{90}$$

Recall that ν_k and λ_k are given from Eqs. (54) and (57), respectively.

When the σ_k do not vary dramatically between the fiber types, which is typically the case, a simple upper estimate of $\eta(\zeta)$ can be made in terms of the minimum value

$$\sigma := \min\{\sigma_k : k = 1, \ldots, N_f\}. \tag{91}$$

Specifically, combining the triangle inequality with the monotonicity of $\frac{1+\mathrm{e}^{-2\lambda_k\sigma_k}}{2\sqrt{\sigma_k^2+\zeta^2}}$ as a function of σ_k gives

$$\begin{aligned}
\eta(\zeta) &\leqslant \left(\sum_{k=1}^{N_f} \gamma_k \frac{\ell_{s_k}}{\lambda_k} \mathrm{e}^{-\sum_{m=1}^{k-1} 2\lambda_m\sigma_m} \frac{1+\mathrm{e}^{-2\lambda_k\sigma_k}}{2\sqrt{\sigma_k^2+\zeta^2}} \right)^2 \\
&\leqslant \left(\sum_{k=1}^{N_f} \gamma_k \frac{\ell_{s_k}}{\lambda_k} \mathrm{e}^{-\sum_{m=1}^{k-1} 2\lambda_m\sigma} \frac{1+\mathrm{e}^{-2\lambda_k\sigma}}{2} \right)^2 \frac{1}{\sigma^2+\zeta^2} \\
&= \Gamma^2 \frac{1}{\sigma^2+\zeta^2},
\end{aligned} \tag{92}$$

where we introduced the worst-case (real) effective nonlinear coefficient

$$\Gamma := \sum_{k=1}^{N_f} \gamma_k \frac{\ell_{s_k}}{\lambda_k} \mathrm{e}^{-\sum_{m=1}^{k-1} 2\lambda_m\sigma} \frac{1+\mathrm{e}^{-2\lambda_k\sigma}}{2} \,. \tag{93}$$

One can think of Γ as arising from a hypothetical situation when the nonlinearities of individual fiber types only face the amount of attenuation of the lowest attenuation fiber and happen to all superpose constructively.

As a consequence, for any non-negative decreasing function $f(\zeta)$ and any ζ_1, we have

$$\frac{1}{\pi}\int_{\zeta_1}^{\zeta_1+\pi} N_s\phi(\zeta) f(\zeta) \mathrm{d}\zeta \leqslant f(\zeta_1) \,. \tag{94}$$

We are ready to estimate $I(\mu,\zeta_0)$, or rather its N_s rescaled version

$$J(\mu,\zeta_0) := N_s I(\mu,\zeta_0) = \int_{\mu}^{\zeta_0} N_s\phi(\zeta) \ln\left(\frac{\zeta_0}{\zeta}\right) \eta(\zeta) \mathrm{d}\zeta \,. \tag{95}$$

Keepig in mind that $\mu = (M+1)\pi$ and $\zeta_0 = (N+1)\pi$ for natural $N > M$, combining inequalities Eqs. (92) and (94) and using the monotonicity of $f(\zeta) := \ln\left(\frac{\zeta_0}{\zeta}\right)\frac{\Gamma^2}{\sigma^2+\zeta^2}$ gives

$$\begin{aligned}
J(\mu,\zeta_0) &= \int_{\mu}^{\zeta_0} N_s\phi(\zeta) \ln(\frac{\zeta_0}{\zeta}) \eta(\zeta) \mathrm{d}\zeta \\
&\leqslant \int_{(M+1)\pi}^{(N+1)\pi} N_s\phi(\zeta) \ln\left(\frac{\zeta_0}{\zeta}\right) \frac{\Gamma^2}{\sigma^2+\zeta^2} \mathrm{d}\zeta \\
&\leqslant \sum_{j=M+1}^{N} \pi \ln\left(\frac{\zeta_0}{\pi j}\right) \frac{\Gamma^2}{\sigma^2+(\pi j)^2} \\
&\leqslant \int_{M\pi}^{N\pi} \ln\left(\frac{\zeta_0}{\zeta}\right) \frac{\Gamma^2}{\sigma^2+\zeta^2} \mathrm{d}\zeta \,.
\end{aligned} \tag{96}$$

Upon setting $\mu' := M\pi = \mu - \pi$ for brevity, the last integral can be integrated by parts

$$\begin{aligned}
\int_{\mu'}^{\zeta_0} \ln\left(\frac{\zeta_0}{\zeta}\right) \frac{1}{\sigma^2+\zeta^2} \mathrm{d}\zeta &= -\ln\left(\frac{\zeta_0}{\mu'}\right)\left[\frac{1}{\sigma}\arctan\left(\frac{\mu'}{\sigma}\right)\right] \\
&+ \int_{\mu'}^{\zeta_0} \frac{1}{\zeta}\left[\frac{1}{\sigma}\arctan\left(\frac{\zeta}{\sigma}\right)\right] \mathrm{d}\zeta.
\end{aligned} \tag{97}$$

By using the crude estimate $\arctan(x) \leqslant \pi/2$, the above expression cannot exceed

$$\begin{aligned}
&-\ln\left(\frac{\zeta_0}{\mu'}\right)\left[\frac{1}{\sigma}\arctan\left(\frac{\mu'}{\sigma}\right)\right] + \frac{\pi}{2\sigma}\int_{\mu'}^{\zeta_0} \frac{1}{\zeta}\mathrm{d}\zeta \\
&= \frac{1}{\sigma}\left[\frac{\pi}{2} - \arctan\left(\frac{\mu'}{\sigma}\right)\right] \ln\left(\frac{\zeta_0}{\mu'}\right) \\
&= \frac{1}{\sigma}\operatorname{arccot}\left(\frac{\mu'}{\sigma}\right) \ln\left(\frac{\zeta_0}{\mu'}\right).
\end{aligned} \tag{98}$$

Looking back at Eq. (96), we have shown that $J(\mu,\zeta_0) \leqslant \Gamma^2 \frac{1}{\sigma}\mathrm{arccot}\left(\frac{\mu'}{\sigma}\right)\ln\left(\frac{\zeta_0}{\mu'}\right)$, which is the promised by Eq. (86a). ■

8.4 Upper bound for $I(0,\delta)$

As a corollary of the above calculations, an upper bound can be found for $I(0,\delta)$. Using that $\sin(2jx) \leqslant 2jx$ (for $x > 0$) in Eq. (81), we have

$$\int_0^{\delta} N_s\phi(\zeta)\mathrm{d}\zeta \leqslant \delta + 2\delta\sum_{j=1}^{N_s-1}\left(1-\frac{j}{N_s}\right) = N_s\delta\,. \quad (99)$$

From Eq. (83), since $\mathrm{Si}(\zeta) \leqslant \min\{\zeta, 2\}$, we have the following inequality:

$$K_{N_s}(\delta) \leqslant \delta + \sum_{j=1}^{N_s-1}\left(\frac{1}{j}-\frac{1}{N_s}\right)\min\{2j\delta, 2\}\,. \quad (100)$$

In particular, choosing $2j\delta$ under the minimum, we get

$$K_{N_s}(\delta) \leqslant \delta + 2\delta\sum_{j=1}^{N_s-1}\left(1-\frac{j}{N_s}\right) = N_s\delta\,. \quad (101)$$

Then, substituting Eqs. (99) and (101) into Eq. (84) and using Eq. (92), we obtain the following bound:

$$I(0,\delta) \leqslant \frac{\Gamma^2}{\sigma^2}\left[\ln\left(\frac{\zeta_0}{\delta}\right)+1\right]\delta\,. \quad (102)$$

9 Result and discussion

In this section, we present an application of the proposed analytical model to the optimal design of a transatlantic coherent optical communications system with hybrid fiber spans composed of two fiber types, a Quasi-Single-Mode Fiber (QSMF)[38,39] and a typical submarine Single-Mode Fiber (SMF). The effective mode area of the fundamental mode for the QSMF is much larger than the one of commercially-available, ultra-low-loss, large-effective-area SMFs. Therefore, launching light in the fundamental mode of the QSMF results in a reduction of the nonlinear distortion during propagation. In practice, however, there is always some random coupling from the fundamental mode to higher-order modes and vice versa because of fiber irregularities. This leads to MPI[27,40]. A trade-off between nonlinear distortion and MPI can be achieved by using hybrid fiber spans composed of QSMF and SMF segments, where the QSMF is placed at the beginning of each span, to reduce most of the nonlinear distortion, followed by the SMF segment, to limit MPI to acceptable levels.

The proposed GN model is used to compute the optimum QSMF/SMF splitting ratio per fiber span. The value of the analytic approach is that it allows us to obtain a fast approximate solution to a problem that would be otherwise too time-consuming to solve numerically. In the following, we check the agreement between the analytical model and Monte Carlo simulation, and we show that the proposed GN model is sufficiently accurate for the determination of the optimum fiber splitting ratio.

9.1 System parameters

We consider a point-to-point link of total length equal to 6000 km, composed of 100 km hybrid fiber spans. The attenuation coefficient of the QSMF (including the excess loss[27]) is 0.16 dB/km and of the SMF is 0.158 dB/km. The effective mode area of the fundamental mode for the QSMF is 250 μm^2 and of the SMF is 112 μm^2. The GVD parameter β_2 is –26.6 ps^2/km for both fiber types. We assume tapered splices between dissimilar optical fibers so that splicing loss is neglected. The EDFA noise figure is 5 dB. We study the propagation of a Nyquist WDM signal composed of 9 wavelength channels, each carrying 32 GBd PDM 16-QAM (QAM means Quadrature Amplitude Modulation).

For modeling the impact of MPI-induced crosstalk, we assume that the QSMF under consideration exhibits weak coupling between the fundamental mode group LP_{01} and the higher-order mode group LP_{11}. For engineering purposes, we assume that MPI can be modeled as a zero-mean, complex Gaussian noise. Then, the MPI coefficient $\tilde{\beta}$ in Eq. (1) can be calculated using power coupled-mode theory[27]. To take into account the impact of MPI compensation in a phenomenological way without actually simulating MPI equalizers, we introduce the MPI compensation level r that varies between zero and one. Then, the MPI coefficient $\tilde{\beta}$ in Eq. (1) is substituted by $\tilde{\beta}(1-r)$.

9.2 Monte Carlo simulation results

Figure 3 shows the variation of Q-factor as a function of the launch power per channel for different fiber configurations, where the QSMF length per span is varied in the range 0–100 km in steps of 5 km. Lines

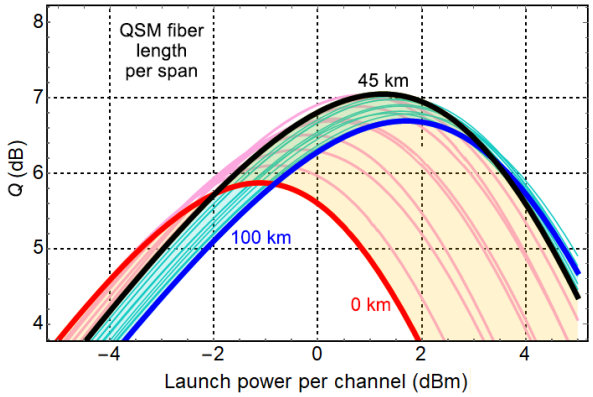

Fig. 3 ***Q*-factor as a function of the total launch power per channel for different QSMF lengths per span (Conditions: System length: 6000 km, 100 km spans; QSMF effective mode area: 250 μm^2; SMF effective mode area: 112 μm^2; No MPI compensation; Lines: Fitting using Eq. (1)).**

represent least-squares fit of Monte Carlo simulation data with Eq. (1), since $Q^2 \sim \mathrm{OSNR}_{\mathrm{eff}}$. Since it is cumbersome to display both the analytical model and the numerical data on the same graph, Monte Carlo simulation points are omitted. To distinguish various simulation cases, we identify individual traces with different colors: fiber configurations with QSMF in the range 0–45 km are shown in pink and the remaining configurations for QSMF in the range 45–100 km per span are shown in cyan. We highlight the extreme cases for 0 km, 45 km, and 100 km of QSMF using thick red, black, and blue lines, respectively.

We observe that the optimum Q-factor increases as the QSMF length per span is increased up to 45 km. For QSMF segments longer than 45 km, the optimum Q-factor gradually declines, eventually reaching approximately a 0.3 dB decrease at 100 km from the peak performance achieved at 45 km.

9.3 Analytical model validation

We shall hereafter focus only on the extreme cases for 0 km, 45 km, and 100 km of QSMF (Fig. 4). We examine two different MPI compensation scenarios:

(1) No MPI compensation at the coherent receiver (Fig. 4a): The optimum Q-factor increases from 5.9 dB for SMF, to 7 dB for 45/55 mix of QSMF/SMF, and then drops to 6.7 dB for QSMF only. In this specific case, the optimum Q-factor is maximized with the use of 45 km QSM fiber per span. The Q-factor improvement

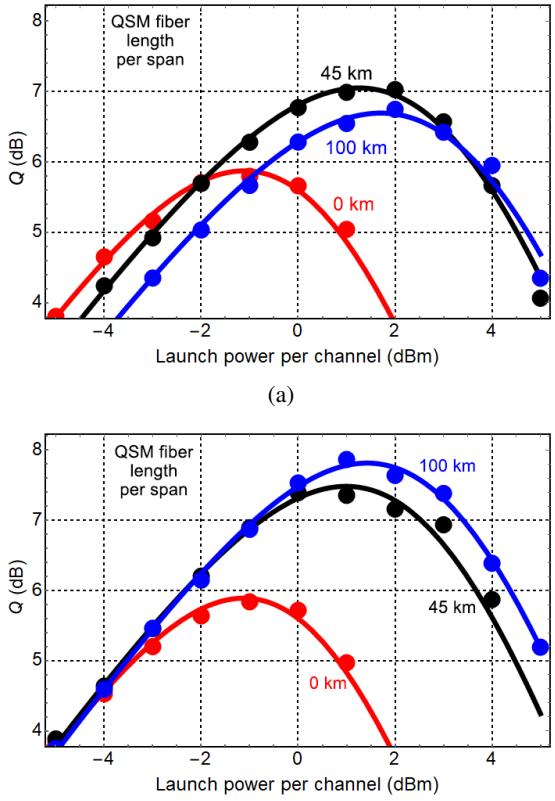

Fig. 4 ***Q*-factor as a function of the total launch power per channel. (a) No MPI compensation and (b) 100% MPI compensation (Points: Monte Carlo simulations; Lines: Fitting using Eq. (1)).**

for using hybrid fiber spans compared to using SMF exclusively is 1.2 dB.

(2) 100% MPI compensation (Fig. 4b): The optimum Q-factor increases from 5.9 dB for SMF, to 7.5 dB for 45/55 mix of QSMF/SMF, to 7.8 dB for QSMF only. In this specific case, the optimum Q-factor is maximized with the exclusive use of QSMF per span. The Q-factor improvement for using only QSMF, compared to using SMF exclusively, is 1.9 dB.

The lines in Fig. 4 are obtained by least squares fitting of the numerical results using Eq. (1), since $Q^2 \sim \mathrm{OSNR}_{\mathrm{eff}}$. Notice that the Monte Carlo simulation points and the fitted lines agree extremely well and this is a strong indication that Eq. (1) is indeed an accurate model. However, we will see in the following that, when $\tilde{\gamma}$ in Eq. (1) is not adjusted by fitting but is analytically calculated instead using the proposed nonlinear GN model, there is a slight mismatch between Eq. (1) and the numerical results.

9.3.1 Q vs. P curves

In the remainder of the paper, we check the accuracy of the proposed nonlinear GN model against Monte Carlo simulation. In the first place, we will show that the proposed nonlinear GN model describes qualitatively the general shape of the simulated Q vs. P curves, but it does not provide pointwise accuracy, especially for higher power levels, where the nonlinear term in the Manakov equation cannot be really considered small and the validity of first-order perturbation theory is questionable. Nevertheless, as we are going to see subsequently, despite its quantitative errors, the proposed nonlinear GN model is sufficient for a quick determination of the optimum fiber splitting ratio.

As an illustration of the disagreement between the proposed nonlinear GN model and the simulation results, we replot from Fig. 4(a) the Monte Carlo simulation points (circles) describing the variation of the Q-factor as a function of the average launch power for the case of 45/55 QSMF/SMF mix in the absence of MPI compensation (Fig. 5). We can vary the agreement between the proposed nonlinear GN model and the simulation results by omitting the phased array term (Eq. (63)) from Eq. (59) and writing instead $\tilde{\gamma} \sim N_s^{1+\epsilon}$, where ϵ is an adjustable parameter[7,9].

In Fig. 5, we superimpose on the same graph the incoherent nonlinear GN model with $\epsilon = 0$ (in blue), the coherent nonlinear GN model (in red), and the partially-coherent nonlinear GN model with $\epsilon = 0.15$ (in black). The analytical models based on coherent and incoherent addition deviate from the numerical results at relatively small launch powers. The peak deviation of the analytical curves in blue and red from the numerical results varies with the fiber attributes and system parameters. In this particular case, if we compare the values at the maxima, there is a mismatch of 0.4 dB between the coherent nonlinear GN model and the simulation. The discrepancy between the analytical and numerical results can be remedied to some extent by using the partially-coherent nonlinear GN model with ϵ as a fitting parameter (black line). However, this would require to run Monte Carlo simulation first in order to select the appropriate value of ϵ by fitting. Fortunately, Fig. 7 below reveals that the coherent nonlinear GN model in itself provides a sufficiently accurate estimate of the optimum fiber splitting ratio, so that it is not necessary to resort to the use of the partially-coherent nonlinear GN model.

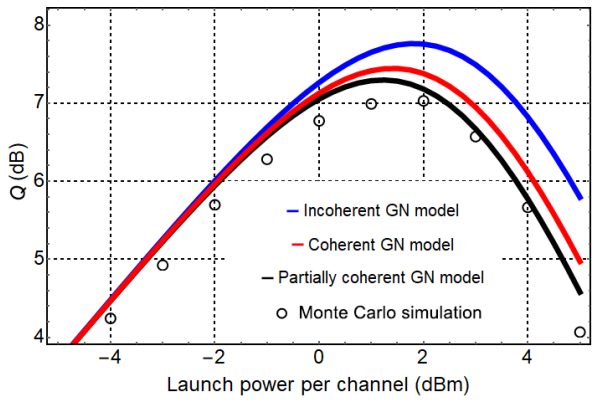

Fig. 5 **Q-factor as a function of the total launch power per channel for the case of 45/55 QSMF/SMF mix (Condition: No MPI compensation).**

9.3.2 Optimum Q-factor vs. QSMF length

As another illustration of the validity of the analytical model, we examine the variation of the peak Q-factor Q_0 as a function of the QSMF length per span (Fig. 6). A major disagreement is apparent. However, we notice

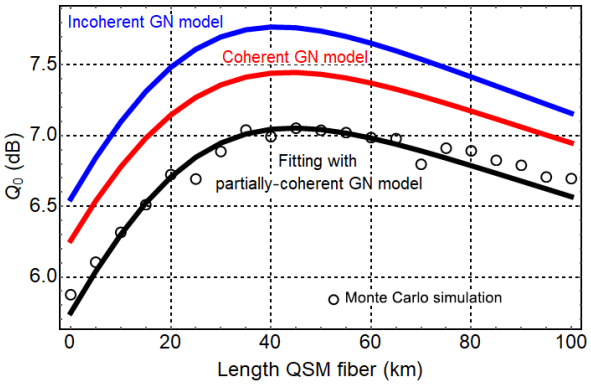

Fig. 6 **Peak Q-factor Q_0 vs. QSMF length ℓ_{s_1} per span (Condition: No MPI compensation).**

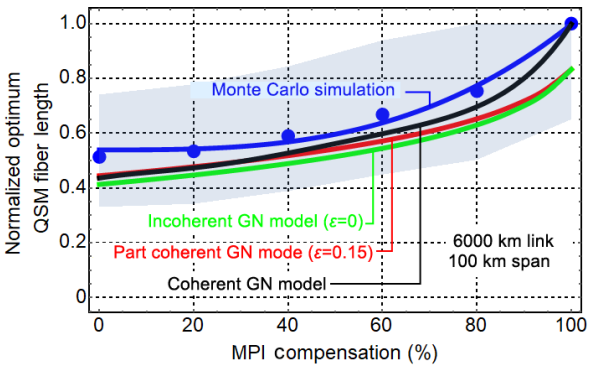

Fig. 7 **Variation of the optimal normalized QSMF length per span ℓ_{s_1}/ℓ_s as a function of the percentage of MPI compensation at the coherent optical receiver.**

that the optimum QSMF length, where the peak Q-factor Q_0 occurs, does not differ substantially from curve to curve. The fact that we obtain essentially the same predictions for the optimum QSMF length from all the different variants of the analytical model is indicative of its usefulness.

9.3.3 Optimum splitting ratio vs. MPI compensation

Figure 7 shows a plot of the optimum length of the QSMF per span ℓ_{s_1} (normalized over the span length ℓ_s) for different levels of MPI compensation. Monte Carlo simulation data are represented by blue points. The blue line shows a phenomenological model fit of the Monte Carlo simulation data. The blue shaded region around the blue line indicates ± 0.1 dB deviations from the optimum Q-values. The other lines show the predictions of different variants of the modified nonlinear GN model. As the MPI compensation level increases, the ratio ℓ_{s_1}/ℓ_s increases to unity. The modified nonlinear GN model predictions are within the blue region.

Besides these validity checks, there are others presented by the authors at ECOC'17[23] for different fiber parameters that corroborate the current findings. Therefore, we believe that we have established the validity of the proposed analytical model for the practical determination of the optimum fiber splitting ratio per span. Henceforth, instead of numerically optimizing the lengths of different fiber segments per span by solving the Manakov equation, which is a time consuming process, one can conveniently resort to the analytical model.

10 Summary

Following the same methodology as the original nonlinear Gaussian noise model for uncompensated coherent optical communications systems with uniform fiber spans[7,9], we provided here an up-to-date and, in some aspects, improved derivation from first principles of an analytical relationship for the nonlinear Gaussian noise variance for hybrid fiber spans. Initially, we restated the full nonlinear Gaussian noise model in just 20 equations based on a synthesis of the literature. While the derivation presented here cannot claim to be fundamentally new, it is somewhat distinct from the one provided in the original publications on the nonlinear Gaussian noise model. Then, we derived new expressions for the nonlinear Gaussian noise variance for systems with multi-segment fiber spans. Even though these formulas were latent in Refs. [7, 9], and the most generic formalism[17], and variants of these formulas were published before, to the best of our knowledge, they were never proven before in their entirety. We hope to bring these formulas to broader attention. The most significant contribution of the current paper is the discussion of the accurate numerical evaluation of the definite integral for the nonlinear Gaussian noise variance, and the development of requisite estimates and asymptotics. Finally, we performed extensive Monte Carlo simulation verification for a representative transatlantic point-to-point link of total length equal to 6000 km with 100 km hybrid fiber spans, composed of an experimental QSMF and a commercially-available, ultra-low-loss, large-effective-area SMF without any splice losses. We showed that the modified nonlinear GN model is sufficiently accurate for the determination of the optimum fiber splitting ratio per span, yielding a system performance within ± 0.1 dB from the optimum Q-value.

Appendix

A List of Greek symbols

β_2	GVD parameter
$\tilde{\beta} P$	Multipath crosstalk variance
γ	Nonlinear coefficient
$\overline{\gamma}$	Averaged nonlinear coefficient $\overline{\gamma} = 8\gamma/9$
$\hat{\gamma}$	Effective nonlinear coefficient
$\tilde{\gamma} P^3$	Nonlinear noise variance
Γ	Worst-case (real) effective nonlinear coefficient
δ	Small number in the vicinity of zero
Δ	Step size of Simpson's quadrature
$\Delta\beta_{ijk}(z)$	Phase mismatch
$\Delta\beta$	Average propagation constant mismatch
$\Delta\nu$	Frequency spacing of WDM channels
$\Delta\nu_{\text{res}}$	Resolution bandwidth
ε	Perturbation parameter
ϵ_r	Relative error
$\eta(f_1, f_2)$, $\eta(\zeta)$	Four-wave mixing efficiency

∂_x	Partial derivative $\partial/\partial x$
λ	Carrier wavelength of central WDM channel
λ_k	WDM channel wavelength
$\overline{\lambda}_k$	Auxiliary multiplicative coefficient
ℓ_s	Span length
ν_k	Normalized electric field attenuation coefficient
σ_k	Normalized, chromatic dispersion-adjusted, and real attenuation coefficient for the k-th fiber segment
$\phi(f_1, f_2), \phi(\zeta)$	Normalized phased-array term
Ψ_m	Set of index triplets for the ODE for the m-th order perturbation
$\xi\,(f_1, f_2)$	Nonlinear noise coefficient integrand
$\zeta_k\,(\zeta)$	Normalized electric field phase shift
Ω_n	Set of index triplets for FWM combinations
ω_n	Angular frequencies, $\omega_n = 2\pi f_n$

B List of English symbols

a	Attenuation coefficient
A_{eff}	Mode effective area
$\overline{a}_{ijk}\,(z)$	Complex attenuation coefficient
$\overline{a}_n$	Complex attenuation coefficient
$\tilde{a}$	ASE noise variance
B_0	Optical bandwidth of the WDM signal
$\boldsymbol{c}_{n0}$	Complex envelope of the unperturbed Fourier coefficient of the n-th spectral component at the fiber input
$\boldsymbol{c}_{n1}$	Complex amplitude of the nonlinear noise
D	Chromatic dispersion parameter
D_x	Regular derivative d/dx
F_A	Amplifier noise figure
f_ϕ	Average phased-array bandwidth
f_{ϕ_k}	Phased-array bandwidth for the k-th fiber segment
f_0	Pseudorandom signal fundamental frequency
G	Amplifier gain
$G_{\text{NLI}}\,(f)$	Nonlinear noise psd
I	Various definite integral
$J(\mu, \zeta_0)$	Auxiliary integral, $J(\mu, \zeta_0) \coloneqq \int_\mu^{\zeta_0} N_s\phi(\zeta)\cdot \ln(\frac{\zeta_0}{\zeta})\eta(\zeta)\mathrm{d}\zeta$
$K_{N_s}(\delta)$	Auxiliary integral, $K_{N_s}(\delta) \coloneqq \int_0^{\delta} \ln(\delta/\zeta)\cdot N_s\phi(\zeta)\mathrm{d}\zeta$
L	Link length
$\hat{L}_{\text{eff}}$	Normalized (i.e., dimensionless) complex effective length
N_{int}	Number of periods of $\phi\,(\zeta)$ in the interval $[0, \zeta_0]$
n_2	Nonlinear index coefficient
N_{ch}	Number of wavelength channels
N_n	Number of integration nodes in a π subinterval
N_s	Number of spans
N_f	Number of fiber segments per span
R	Region of integration in the hyperbolic uv-plane
T_0	Pseudorandom signal period
X_{ijk}, X_{ij}	Complex FWM efficiency
$x_k\,(\zeta)$	Normalized power complex attenuation coefficients
$\boldsymbol{u}_n(z)$	Fourier coefficients
$\boldsymbol{u}_{nk}(z)\varepsilon^k$	k-th order correction to the unperturbed solution $\boldsymbol{u}_{n0}(z)$
$\boldsymbol{y}(z, t)$	Complex envelope WDM PDM signal

References

[1] G. P. Agrawal, *Nonlinear Fiber Optics*, 5th ed. Academic Press, 2012.

[2] P. K. A. Wai and C. R. Menyuk, Polarization mode dispersion, decorrelation, and diffusion in optical fibers with randomly varying birefringence, *J. Lighttw. Technol.*, vol. 14, no. 2, pp. 148–157, 1996.

[3] X. Chen and W. Shieh, Closed-form expressions for nonlinear transmission performance of densely spaced coherent optical OFDM systems, *Opt. Express*, vol. 18, no. 18, pp. 19 039–19 054, 2010.

[4] W. Shieh and X. Chen, Information spectral efficiency and launch power density limits due to fiber nonlinearity for coherent optical ofdm systems, *IEEE Photonics Journal*, vol. 3, no. 2, pp. 158–173, 2011.

[5] P. Poggiolini, A. Carena, V. Curri, G. Bosco, and F. Forghieri, Analytical modeling of nonlinear propagation in uncompensated optical transmission links, *IEEE Photon. Technol. Lett.*, vol. 23, no. 11, pp. 742–744, 2011.

[6] A. Carena, V. Curri, G. Bosco, P. Poggiolini, and F. Forghieri, Modeling of the impact of nonlinear propagation effects in uncompensated optical coherent transmission links, *J. Lighttw. Technol.* vol. 30, no. 10, pp. 1524–1539, 2012.

[7] P. Poggiolini, The GN model of non-linear propagation in uncompensated coherent optical systems, *J. Lightwave Technol.*, vol. 30, no. 24, pp. 3857–3879, 2012.

[8] P. Johannisson and M. Karlsson, Perturbation analysis of nonlinear propagation in a strongly dispersive optical communication system, *J. Lighttw. Technol.*, vol. 31, no. 8, pp. 1273–1282, 2013.

[9] P. Poggiolini, G. Bosco, A. Carena, V. Curri, Y. Jiang, and F. Forghieri, The GN-model of fiber non-linear propagation and its applications, *J. Lightwave Technol.*, vol. 32, no. 4, pp. 694–721, 2014.

[10] A. Mecozzi and R. J. Essiambre, Nonlinear Shannon limit in pseudolinear coherent systems, *J. Lighttw. Technol.*, vol. 30, no. 12, pp. 2011–2024, 2012.

[11] R. Dar, M. Feder, A. Mecozzi, and M. Shtaif, Properties of nonlinear noise in long, dispersion-uncompensated fiber links, *Opt. Express*, vol. 21, no. 22, pp. 25 685–25 699, 2013.

[12] A. Carena, G. Bosco, V. Curri, Y. Jiang, P. Poggiolini, and F. Forghieri, EGN model of non-linear fiber propagation, *Opt. Express*, vol. 22, no. 13, pp. 16 335–16 362, 2014.

[13] P. Serena and A. Bononi, A time-domain extended Gaussian noise model, *J. Lighttw. Technol.*, vol. 33, no. 7, pp. 1459–1472, 2015.

[14] A. Ghazisaeidi, A theory of nonlinear interactions between signal and amplified spontaneous emission noise in coherent wavelength division multiplexed systems, *J. Lightwave Technol.*, vol. 35, no. 23, pp. 5150–5175, 2017.

[15] V. Curri, A. Carena, P. Poggiolini, G. Bosco, and F. Forghieri, Extension and validation of the GN model for non-linear interference to uncompensated links using Raman amplification, *Opt. Express*, vol. 21, no. 3, pp. 3308–3317, 2013.

[16] P. Poggiolini and Y. Jiang, Recent advances in the modeling of the impact of nonlinear fiber propagation effects on uncompensated coherent transmission systems, *J. Lightwave Technol.*, vol. 35, no. 3, pp. 458–480, 2017.

[17] D. Semrau, R. I. Killey, and P. Bayvel, The Gaussian noise model in the presence of inter-channel stimulated Raman scattering, *J. Lighttw. Technol.*, vol. 36, no. 14, pp. 3046–3055, 2018.

[18] H. Rabbani, G. Liga, V. Oliari, L. Beygi, E. Agrell, M. Karlsson, and A. Alvarado, A general analytical model of nonlinear fiber propagation in the presence of Kerr nonlinearity and stimulated Raman scattering, arXiv preprint arXiv:1909.08714, 2019.

[19] P. Poggiolini, A closed-form GN-model non-linear interference coherenceterm, arXiv preprint arXiv:1906.03883, 2019.

[20] M. Ranjbar Zefreh and P. Poggiolini, A GN-model closed-form formula considering coherency terms in the link function and covering all possible islands in 2-D GN integration, arXiv preprint arXiv:1907.09457, 2019.

[21] M. Ranjbar Zefreh and P. Poggiolini, A closed-form approximate incoherent GN-model supporting MCI contributions, arXiv preprint arXiv:1911.03321, 2019.

[22] J. D. Downie, M. Mlejnek, I. Roudas, W. A. Wood, A. Zakharian, J. E. Hurley, S. Mishra, F. Yaman, S. Zhang, E. Ip, and Y. K. Huang, Quasi-single-mode fiber transmission for optical communications, *IEEE J. Sel. Top. Quantum Electron.*, vol. 23, no. 3, pp. 1–12, 2017.

[23] L. Miranda, I. Roudas, J. D. Downie, and M. Mlejnek, Performance of coherent optical communication systems with hybrid fiber spans, in *Proc. of Eur. Conf. Opt. Commun.* (*ECOC*), Gothenburg, Sweden, 2017, p. P2.SC6.18.

[24] M. A. Z. Al-Khateeb, M. A. Iqbal, M. Tan, A. Ali, M. McCarthy, P. Harper, and A. D. Ellis, Analysis of the nonlinear Kerr effects in optical transmission systems that deploy optical phase conjugation, *Opt. Express*, vol. 26, no. 3, pp. 3145–3160, 2018.

[25] L. Krzczanowicz, M. A. Z. Al-Khateeb, M. A. Iqbal, I. Phillips, P. Harper, and W. Forysiak, Performance estimation of discrete Raman amplification within broadband optical networks, in *Proc. of Opt. Fiber Commun. Conf.* (*OFC*), *2019*, San Diego, CA, USA, 2019, p. Tu3F.4.

[26] A. Bononi, O. Beucher, and P. Serena, Single- and cross-channel nonlinear interference in the gaussian noise model with rectangular spectra, *Opt. Express*, vol. 21, no. 26, pp. 32 254–32 268, 2013.

[27] M. Mlejnek, I. Roudas, J. D. Downie, N. Kaliteevskiy, and K. Koreshkov, Coupled-mode theory of multipath interference in quasi-single mode fibers, *IEEE Photon. J.*, vol. 7, no. 1, pp. 1–16, 2015.

[28] A. H. Nayfeh, *Perturbation Methods*. Wiley, 2008.

[29] C. M. Bender and S. A. Orszag, *Advanced mathematical methods for scientists and engineers I*: *Asymptotic methods and perturbation theory*. Springer, 2013.

[30] J. Proakis and M. Salehi, *Digital Communications*, 5th ed. McGraw-Hill, 2007.

[31] E. Forestieri and M. Secondini, Solving the nonlinear Schrödinger equation, in *Optical Communication Theory and Techniques*, E. Forestieri, ed. Springer, 2005, pp. 3–11.

[32] W. Rudin, *Real and Complex Analysis, 3rd Ed.* McGraw-Hill, 1987.

[33] G. P. Agrawal, *Fiber-Optic Communication Systems*, 4th ed. Wiley, 2010.

[34] S. Olver, Numerical approximation of highly oscillatory integrals, PhD dissertation, University of Cambridge, Cambridge, UK, 2008.

[35] H. Anton and A. Herr, *Calculus with Analytic Geometry*. Wiley, 1995.

[36] Wolfram Research Inc., Mathematica 12.0, http://

www.wolfram.com, 2019.

[37] Fejér kernel—Wikipedia, the free encyclopedia, https://en.wikipedia.org/w/index.php?title=Fej%C3%A9r_kernel&oldid=850230465, 2018.

[38] J. D. Downie, M. J. Li, M. Mlejnek, I. G. Roudas, W. A. Wood, and A. R. Zakharian, Optical transmission systems and methods using a QSM large-effective-area optical fiber, US Patent 9 841 555, Dec. 12, 2017.

[39] M. J. Li, S. K. Mishra, M. Mlejnek, W. A. Wood, and A. R. Zakharian, Quasi-single-mode optical fiber with a large effective area, U.S. Patent 9 846 275, Dec. 19, 2017.

[40] Q. Sui, H. Zhang, J. D. Downie, W. A. Wood, J. Hurley, S. Mishra, A. P. T. Lau, C. Lu, H. Y. Tam, and P. K. A. Wai, Long-haul quasi-single-mode transmissions using few-mode fiber in presence of multi-path interference, *Opt. Express*, vol. 23, no. 3, pp. 3156–3169, 2015.

Ioannis Roudas received the BS degree in physics and the MS degree in electronics and radio-engineering from the University of Athens, Greece in 1988 and 1990, respectively, and the MS and PhD degrees in coherent optical communication systems from the Ecole Nationale Supérieure des Télécommunications (currently Télécom ParisTech), Paris, France in 1991 and 1995, respectively. During 1995–1998, he worked in the Optical Networking Research Department, Bell Communications Research (Bellcore), Red Bank, NJ. At the same time, he taught for two semesters, as an adjunct professor, at Columbia University. He was subsequently with the Photonic Modeling and Process Engineering Department, Corning Inc., Somerset, NJ, from 1999 to 2002. He spent an eight-year period in Greece, during 2003–2011, working at the Department of Electrical and Computer Engineering, University of Patras as an associate professor of optical communications. In addition, he taught, as an adjunct professor, at the City University of New York and the Hellenic Open University. During 2011–2016, he was a research associate with the Science and Technology Division of Corning Inc., Corning, NY. Since July 2016, he has been with the Department of Electrical and Computer Engineering, Montana State University as the Gilhousen Telecommunications chair professor. He is the author or co-author of more than 100 papers in scientific journals and international conferences and holds five patents. He served as an associate editor for the *IEEE Photonics Journal* during 2013–2019. His current research focuses on optical communications systems with multimode and multicore fibers and on quantum networking.

Jaroslaw Kwapisz is a Polish-American mathematician with background in theoretical dynamical systems. He received the MS (1991) degree from University of Warsaw and the PhD degree (1995) from State University of New York at Stony Brook. Since July 2008, he has been a professor of mathematics at the Department of Mathematical Sciences, Montana State University. He has worked on problems in several subject areas, including integral and differential equations, iterated maps modeling coupled non-linear oscillators, pattern formation in fourth-order Hamiltonian systems, ergodic theory and entropy in smooth and symbolic dynamics, cohomological Conley index and cocyclic subshifts, almost-periodic tiling spaces and quasi-crystals, abelian-Nielsen classes and geometry of translation surfaces, and conformal dimension of fractal sets. He is currently interested in Anosov maps on infra-nil manifolds, non-Meyer substitution Delone sets, and problems in classical and quantum multi-mode fiber-optic communication.

Xin Jiang received the BS, MS, and PhD degrees in electronic engineering from Tsinghua University, Beijing, China, the former one in 1990, and the later two in 1995. She is currently an associate professor at the Department of Engineering and Environmental Science, College of Staten Island (CSI), City University of New York, NY, USA. Prior joining CSI, she has worked in R&D and engineering departments of several high-tech and telecommunication companies. She has authored and co-authored over 60 publications in peer-reviewed journals and international conferences. Her current areas of research include advanced optical fiber transmission technology and photonic systems and networks.